**THE EUROPEAN
PHYSICAL JOURNAL C**

Measurement of D-meson production at mid-rapidity in pp collisions at $\sqrt{s} = 7$ TeV

ALICE Collaboration[*]

CERN, 1211 Geneva 23, Switzerland

Abstract The production cross sections for prompt charmed mesons D^0, D^+, D^{*+} and D_s^+ were measured at mid-rapidity in proton–proton collisions at a centre-of-mass energy $\sqrt{s} = 7$ TeV with the ALICE detector at the Large Hadron Collider (LHC). D mesons were reconstructed from their decays $D^0 \to K^-\pi^+$, $D^+ \to K^-\pi^+\pi^+$, $D^{*+} \to D^0\pi^+$, $D_s^+ \to \phi\pi^+ \to K^-K^+\pi^+$, and their charge conjugates. With respect to previous measurements in the same rapidity region, the coverage in transverse momentum (p_T) is extended and the uncertainties are reduced by a factor of about two. The accuracy on the estimated total $c\bar{c}$ production cross section is likewise improved. The measured p_T-differential cross sections are compared with the results of three perturbative QCD calculations.

1 Introduction

In high-energy hadronic collisions heavy quarks are produced by hard scatterings between partons of the two incoming hadrons. The production cross section of hadrons with charm or beauty quarks is calculated in the framework of Quantum Chromodynamics (QCD) and factorised as a convolution of the hard scattering cross sections at partonic level, the parton distribution functions (PDFs) of the incoming hadrons and the non-perturbative fragmentation functions of heavy quarks to heavy-flavour hadrons. Factorisation is implemented in terms of the squared momentum transfer Q^2 (collinear factorisation) [1] or of the partonic transverse momentum k_T [2]. The hard scattering cross section is expanded in a perturbative series in powers of the strong coupling constant α_s. State-of-the-art calculations based on collinear factorisation implement a perturbative expansion up to next-to-leading order (NLO) in α_s, such as the general-mass variable flavour number scheme (GM-VFNS) [3–5], or next-to-leading order in α_s with all-order resummation of the logarithms of p_T/m_Q (FONLL) [6,7], where p_T and m_Q are the heavy-quark transverse momentum and mass,

respectively. Calculations based on k_T factorisation exist only at leading order (LO) in α_s [2,8,9]. All these calculations provide a good description of the production cross sections of D and B mesons in proton–proton (and proton–antiproton) collisions at centre-of-mass energies from 0.2 to 13 TeV over a wide p_T range at both central and forward rapidities (see e.g. [10] and references therein). In the case of charm production the uncertainties of the theoretical calculations, dominated by the perturbative scale uncertainties, are significantly larger than the experimental ones [11–21]. However, it was recently pointed out that in ratios of cross sections at different LHC energies and in different rapidity intervals the perturbative uncertainty becomes subdominant with respect to the uncertainty on the PDFs [22], thus making the measurement sensitive in particular to the gluon PDF at values of Bjorken-x down to 10^{-5} when the D-meson p_T approaches 0. This represents a strong motivation for pursuing precise measurements of D-meson production in pp collisions at LHC energies. Charm hadroproduction measurements are also required for cosmic-ray and neutrino astrophysics, where high-energy neutrinos from the decay of charmed hadrons produced in particle showers in the atmosphere constitute an important background for neutrinos from astrophysical sources [23–26].

In the context of the heavy-ion programme at the LHC, D-meson measurements in pp collisions represent an essential reference for the study of effects induced by cold and hot strongly-interacting matter in the case of proton–nucleus and nucleus–nucleus collisions (see e.g. the recent reviews [10, 27]). In addition, the $c\bar{c}$ production cross section per nucleon–nucleon collision is a basic ingredient for the determination of the amount of charmonium production by (re)generation in a quark-gluon plasma [28–30], a mechanism that is supported by J/ψ measurements in nucleus–nucleus collisions at the LHC [31,32]. A precise measurement of the $c\bar{c}$ production cross section in pp collisions would enable a more stringent comparison of model calculations with data.

In this article, we report the measurement of the production cross sections of prompt D^0, D^+, D^{*+} and D_s^+

[*] e-mail: alice-publications@cern.ch

Springer

mesons (as average of particles and anti-particles), and of their ratios, in pp collisions at the centre-of-mass energy $\sqrt{s} = 7$ TeV using the ALICE detector at the LHC. The measurements cover mid-rapidity ($|y| < 0.5$) and the intervals $0 < p_T < 36$ GeV/c for D^0 mesons, $1 < p_T < 24$ GeV/c for D$^+$ and D^{*+}mesons, and $2 < p_T < 12$ GeV/c for D$_s^+$ mesons. The measurements cover complementary intervals in p_T and rapidity with respect to those published by the ATLAS ($3.5 < p_T < 100$ GeV/c, $|\eta| < 2.1$ [13]) and LHCb ($0 < p_T < 8$ GeV/c, $2 < y < 4.5$ [19]) Collaborations at the same centre-of-mass energy. In comparison to previous ALICE publications based on the same data sample [14,16,17], the present results have a significantly extended p_T coverage (for example, the previous coverage for D^0 mesons was 0–16 GeV/c) and total uncertainties reduced by a factor of about two. These improvements have several sources: (i) changes in the detector calibration, alignment and track reconstruction algorithm, which resulted in better p_T resolution, thus higher signal-to-background ratio; (ii) optimization of the D-meson selection procedure; (iii) refinements in the estimation of the systematic uncertainties, which is now more data-driven; (iv) a data sample with 20% larger integrated luminosity.

The article is organised as follows: the data sample and the analysis procedure are described in Sect. 2, the estimation of the systematic uncertainties is discussed in Sect. 3 and the results are presented and compared to theoretical calculations in Sect. 4.

2 Analysis

A complete description of the ALICE experimental setup and of its performance can be found in [33,34]. D mesons were reconstructed at mid-rapidity from their decay products, using the tracking and particle identification capabilities of the ALICE central barrel detectors located within a large solenoidal magnet, providing a field B = 0.5 T parallel to the beam line (z axis of the ALICE reference frame). The innermost detector, the Inner Tracking System (ITS), is used to track charged particles within the pseudorapidity interval $|\eta| < 0.9$ as well as for primary and secondary vertex reconstruction. It consists of six cylindrical layers equipped with Silicon Pixel Detectors (SPD), Silicon Drift Detectors (SDD) and Silicon Strip Detectors (SSD) from inner to outer layers. The ITS provides a resolution on the track impact parameter d_0 to the primary vertex in the transverse plane ($r\varphi$) better than 75 μm for transverse momentum $p_T > 1$ GeV/c. As compared to previous publications based on the same data sample [14,16], the alignment of the ITS sensor modules was improved and a new procedure for the calibration of the drift velocity and of the non-uniformities of the drift field in the SDD was used. The Time Projection Chamber (TPC)

provides track reconstruction as well as particle identification via the measurement of the specific ionisation energy loss dE/dx. The Time-Of-Flight detector (TOF) extends the charged particle identification capabilities of the TPC via the measurement of the flight time of the particles from the interaction point. The event collision time is measured with the T0 detector, which consists of two arrays of Cherenkov counters located at +350 cm and −70 cm along the beam line, or, for the events with sufficiently large multiplicity, it is estimated using the particle arrival times at the TOF [35]. The V0 detector, used in the online trigger and offline event selection, consists of two arrays of 32 scintillators each, covering the pseudorapidity intervals $-3.7 < \eta < -1.7$ and $2.8 < \eta < 5.1$, placed around the beam vacuum tube on either side of the interaction region. A minimum-bias (MB) trigger was used to collect the data sample, by requiring at least one hit in either of the V0 counters or in the SPD ($|\eta| < 2$). Events were selected off-line by using the timing information from the V0 and the correlation between the number of hits and track segments in the SPD detector to remove background due to beam–gas interactions. Only events with a primary vertex reconstructed within ±10 cm from the centre of the detector along the beam line were used for the analysis. The analysed data sample consists of about 370 million MB events, corresponding to an integrated luminosity $L_{int} = (6.0 \pm 0.2)$ nb^{-1}, collected during the 2010 pp run at $\sqrt{s} = 7$ TeV.

D mesons were reconstructed via their hadronic decay channels D$^0 \to$ K$^-\pi^+$ (with branching ratio, BR = 3.93 ± 0.04%), D$^+ \to$ K$^-\pi^+\pi^+$ (BR = 9.46 ± 0.24%), D^{*+}(2010) $\to$ D$^0\pi^+$ (strong decay with BR = 67.7 ± 0.5%) with D$^0 \to$ K$^-\pi^+$ and D$_s^+ \to \phi\pi^+$ with $\phi \to$ K$^-$K$^+$ (BR = 2.27 ± 0.08%), together with their charge conjugates [36].

D-meson candidates were defined using pairs or triplets of tracks with the proper charge-sign combination. Tracks were required to have $|\eta| < 0.8$, $p_T > 0.3$ GeV/c, at least 70 associated TPC space points (out of a maximum of 159), χ^2/ndf < 2 in the TPC (where ndf is the number of degrees of freedom involved in the track fit procedure), and at least one hit in either of the two layers of the SPD. For the soft pion produced in D^{*+} decay, also tracks reconstructed only with the ITS, with at least four hits, including at least one in the SPD, and $p_T > 80$ MeV/c were considered. With these track selection criteria, the acceptance in rapidity for D mesons drops steeply to zero for $|y| > 0.5$ at low p_T and $|y| > 0.8$ at $p_T > 5$ GeV/c. A p_T-dependent fiducial acceptance cut was therefore applied on the D-meson rapidity, $|y| < y_{fid}(p_T)$, with $y_{fid}(p_T)$ increasing from 0.5 to 0.8 in the transverse momentum range $0 < p_T < 5$ GeV/c according to a second-order polynomial function, and $y_{fid} = 0.8$ for $p_T > 5$ GeV/c.

D^0, D$^+$ and D$_s^+$ mesons have mean proper decay lengths $c\tau$ of about 123, 312 and 150 μm, respectively [36]. Their decay vertices are therefore typically displaced by a few hun-

dred μm from the primary vertex of the interaction. Geometrical selections on the D-meson decay topology were applied to reduce the combinatorial background. The selection requirements were tuned so as to provide a large statistical significance for the signal and to keep the selection efficiency as high as possible. The latter requirement was dictated also by the fact that too tight cuts result in an increased contribution to the raw yield from feed-down D mesons originating from decays of B mesons. In the $D^{*+} \rightarrow D^0\pi^+$ case, the decay vertex cannot be resolved from the primary vertex and geometrical selections were applied on the secondary vertex topology of the produced D^0. The geometrical selections were mainly based on the displacement of the tracks from the interaction vertex, the distance between the D-meson decay vertex and the primary vertex (decay length, L), and the pointing of the reconstructed D-meson momentum to the primary vertex. The pointing condition is applied by requiring a small value for the angle θ_{pointing} between the directions of the reconstructed momentum of the candidate and its flight line, defined by the vector from the primary to the secondary vertex. In comparison to the previous analysis of the same data sample, additional selection criteria were introduced. In particular, the projections of the pointing angle and of the decay length in the transverse plane ($\theta^{r\varphi}_{\text{pointing}}$ and $L^{r\varphi}$) were considered. Moreover, a cut on the normalised difference between the measured and expected impact parameters of each of the decay particles ($d_{0,\text{tr}}^{\text{reco}} - d_{0,\text{tr}}^{\text{exp}})/\sigma_\Delta$ was applied, where $d_{0,\text{tr}}^{\text{reco}}$ is the measured track impact parameter, $d_{0,\text{tr}}^{\text{exp}}$ is defined as $L^{r\varphi} \sin(\theta^{r\varphi}_{\text{tr,D}})$, $\theta^{r\varphi}_{\text{tr,D}}$ is the measured angle between the momenta of the D meson and of the considered track, and σ_Δ is the combination of the uncertainties on the measured and expected d_0. By requiring $(d_{0,\text{tr}}^{\text{reco}} - d_{0,\text{tr}}^{\text{exp}})/\sigma_\Delta < 3$, a significant rejection of background candidates (15–40% depending on D-meson species and p_T) and feed-down D mesons (up to 50% at high p_T) is achieved while keeping almost 100% of the prompt D mesons.

Further reduction of the combinatorial background was obtained by applying particle identification (PID) to the decay tracks. A 3σ compatibility cut was applied on the difference between the measured and expected signals for pions and kaons for both the dE/dx and time-of-flight. Tracks without TOF hits were identified using only the TPC information with a 3σ selection for D^0, D^+ and D^{*+} decay products, and a 2σ selection for the D_s^+. This stricter PID selection strategy was needed in the D_s^+ case due to the large background of track triplets and the short D_s^+ lifetime, which limits the effectiveness of the geometrical selections on the displaced decay-vertex topology. Based on the PID information and the charge sign of the decay tracks, D^0 candidates were accepted (as D^0, $\overline{D^0}$, or both) or rejected, according to the compatibility with the $K^\mp \pi^\pm$ final state. For the D^{*+} reconstruction, this ambiguity is resolved using the charge of the soft pion. In the cases of the $D_s^+ \rightarrow K^-K^+\pi^+$ and

$D^+ \rightarrow K^-\pi^+\pi^+$ decays, a candidate was rejected if the track with charge opposite to that of the D meson was not compatible with the kaon PID hypothesis.

The D-meson raw yields, including both particles and antiparticles, were obtained from fits to the D^0, D^+ and D_s^+ candidate invariant-mass distributions and to the mass difference $\Delta M = M(K\pi\pi) - M(K\pi)$ distributions for D^{*+} candidates. In the fit function, the signal was modeled with a Gaussian and the background was described by an exponential term for D^0, D^+ and D_s^+ candidates and by the function $a\sqrt{\Delta M - m_\pi} \cdot e^{b(\Delta M - m_\pi)}$ for D^{*+} candidates. In the case of D^0 mesons, an additional term was included in the fit function to account for the contribution of signal candidates that are present in the invariant mass distribution with the wrong daughter particle mass assignment (reflections). A study with Monte Carlo simulations showed that about 70% of these reflections are rejected by the PID selections. The residual contribution was accounted for by including in the fit a template consisting of the sum of two wide Gaussians with centroids and widths fixed to values obtained in the simulation and with amplitudes normalised using the signal observed in data.

Figure 1 shows fits to the invariant-mass (mass-difference) distributions in three p_T intervals for D^0, D^+, (D^{*+}) and D_s^+ candidates from top to bottom. The mean values of the Gaussians in all transverse-momentum intervals were found to be compatible within uncertainties with the world average rest mass values for D^0, D^+ and D_s^+ and with the difference $M_{D^{*+}} - M_{D^0}$ for the D^{*+} [36]. The widths are consistent with the results from Monte Carlo simulations and smaller by 10–20% than the values in [14,16], as a consequence of the improved p_T resolution.

The p_T-differential cross section of prompt D mesons was computed as:

$$\frac{\mathrm{d}^2\sigma^D}{\mathrm{d}p_T\mathrm{d}y} = \frac{1}{c_{\Delta y}\,\Delta p_T}\frac{1}{\mathrm{BR}}\frac{\frac{1}{2}\,f_{\text{prompt}}\cdot N^{D+\overline{D},\text{raw}}\Big|_{|y|<y_{\text{fid}}}}{(\text{Acc}\times\varepsilon)_{\text{prompt}}}\frac{1}{L_{\text{int}}},$$
(1)

where f_{prompt}, $N^{D+\overline{D},\text{raw}}$ and $(\text{Acc}\times\varepsilon)_{\text{prompt}}$ are p_T-interval dependent quantities. The raw yield values (sum of particles and antiparticles, $N^{D+\overline{D},\text{raw}}$) were corrected for the B-meson decay feed-down contribution (i.e. multiplied by the prompt fraction f_{prompt} in the raw yield), divided by the acceptance-times-efficiency for prompt D mesons $(\text{Acc}\times\varepsilon)_{\text{prompt}}$, and divided by a factor of two to obtain the particle and antiparticle averaged yields. The p_T-differential yields for each D-meson species, measured separately for particles and antiparticles, were found to be in agreement within statistical uncertainties. The corrected yields were divided by the decay channel BR, the p_T interval width Δp_T, the correction factor for the rapidity coverage $c_{\Delta y}$, and the integrated luminosity $L_{\text{int}} = N_{\text{ev}}/\sigma_{\text{MB}}$, where N_{ev} is the number of analysed
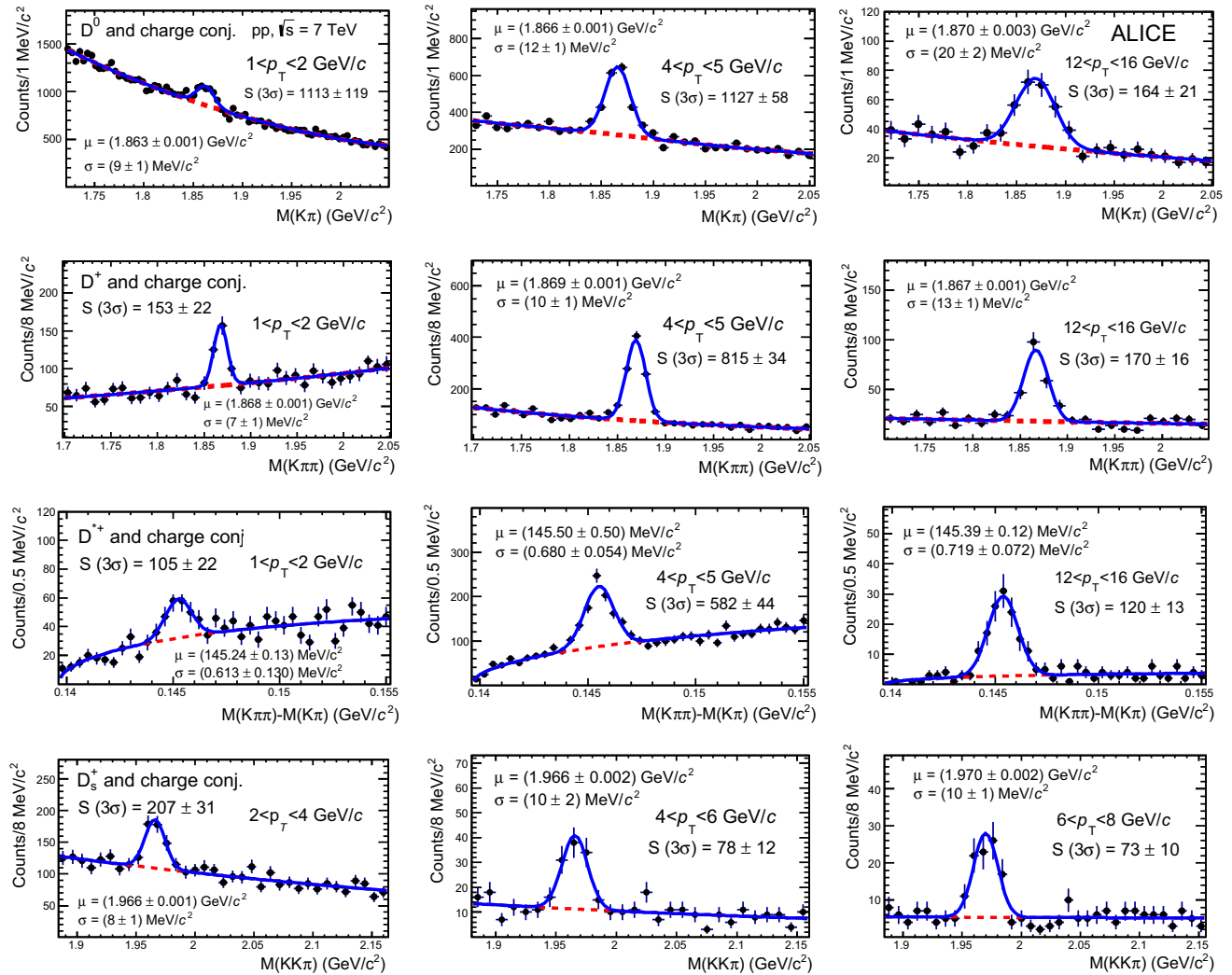
Fig. 1 Invariant-mass (mass-difference) distributions of D^0, D^+, (D^{*+}) and D_s^+ candidates and charge conjugates in three p_T intervals for a sample of pp collisions at $\sqrt{s} = 7$ TeV with $L_{int} = 6.0$ nb^{-1}. The *curves* show the fit functions as described in the text. The contribution of reflections for the D^0 meson is included. The values of mean (μ) and width (σ) of the signal peak are reported together with the signal counts (S) in the mass interval ($\mu - 3\sigma$, $\mu + 3\sigma$)

events and $\sigma_{MB} = 62.2$ mb is the cross section for the MB trigger condition [37].

The (Acc $\times \varepsilon$) correction factor was determined using simulations of pp collisions generated with the PYTHIA 6.4.21 event generator [38] (Perugia-0 tune [39]), and particle transport through the apparatus using GEANT3 [40]. The luminous region distribution and the conditions of all the ALICE detectors were included in the simulations. The (Acc $\times \varepsilon$) for prompt and feed-down D^0, D^+, D^{*+} and D_s^+ mesons with $|y| < y_{fid}$ is shown in Fig. 2 as a function of p_T. The efficiencies for feed-down D mesons are higher than those for prompt D mesons in most of the p_T intervals, because the decay vertices of the feed-down D mesons are on average more displaced from the primary vertex due to the large B-meson lifetime ($c\tau \approx 500$ µm [36]). However, the selection

on the difference between measured and expected decay-track impact parameters rejects more efficiently feed-down D mesons, thus reducing the difference between prompt and feed-down efficiencies as compared to the previous analyses.

The rapidity acceptance correction factor $c_{\Delta y}$ was computed with the PYTHIA 6.4.21 event generator with Perugia-0 tune as the ratio between the generated D-meson yield in $\Delta y = 2 y_{fid}$, (with y_{fid} varying from 0.5 at low p_T to 0.8 at high p_T) and that in $|y| < 0.5$. It was checked that calculations of the $c_{\Delta y}$ correction factor based on FONLL pQCD calculations [7] or on the assumption of uniform D-meson rapidity distribution in $|y| < y_{fid}$ would give the same result, because both in PYTHIA and in FONLL the D-meson yield is uniform within 1% in the range $|y| < 0.8$.
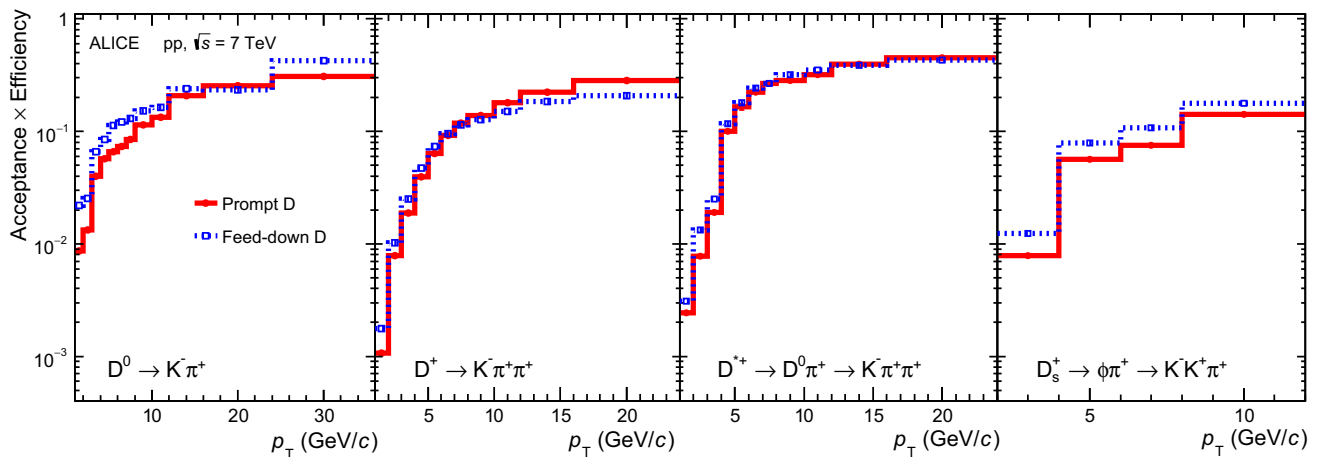
Fig. 2 Acceptance × efficiency for D^0, D^+, D^{*+} and D_s^+ mesons, as a function of p_T. The efficiencies for prompt (*solid lines*) and feed-down (*dotted lines*) D mesons are shown

The f_{prompt} fraction was calculated using the B production cross sections from FONLL calculations [6,41], the B $\rightarrow$ D + X decay kinematics from the EvtGen package [42] and the efficiencies for feed-down D mesons reported in Fig. 2:

$$f_{prompt} = 1 - \frac{N_{raw}^{D\,feed\text{-}down}}{N_{raw}^{D}} = 1 - \left(\frac{d^2\sigma}{dp_T dy}\right)^{FONLL}_{feed\text{-}down}$$
$$\cdot \frac{(Acc \times \varepsilon)_{feed\text{-}down} \cdot c_{\Delta y}\Delta p_T \cdot BR \cdot L_{int}}{N^{D+\overline{D},raw}/2}, \quad (2)$$

where the p_T dependence of f_{prompt}, $N^{D+\overline{D},raw}$ and (Acc × ε)$_{feed\text{-}down}$ is omitted for brevity. The values of f_{prompt} range between 0.85 and 0.97 depending on D-meson species and p_T.

3 Systematic uncertainties

Systematic uncertainties were estimated considering several sources. A summary is shown in Table 1 for two p_T intervals. New or refined procedures were used with respect to the analyses presented in [14,16], in particular for the uncertainties on the signal yield extraction, the track reconstruction efficiency and the feed-down subtraction.

The systematic uncertainties on the yield extraction obtained from the fits to the invariant-mass distributions (mass difference for D^{*+} mesons) were evaluated by repeating the fits several times varying (i) the invariant-mass bin width, (ii) the lower and upper limits of the fit range, (iii) the background fit function (exponential function, first, second and third order polynomials were used for D^0, D^+ and D_s^+ and a power law for the D^{*+}), for a total of about few hundred fits for each D-meson species and p_T interval. In addition, the same approach was used with a bin counting method, in which the signal yield was obtained by integrating the invariant-mass distribution after subtracting the background estimated from a fit to the side-bands. The distributions of the signal yield obtained from these variations are consistent with a Gaussian shape and the mean of the distributions is close to the central value of the yield. The systematic uncertainty was defined as the R.M.S. of this distribution.

The systematic uncertainty on the track reconstruction efficiency was estimated by varying the track-quality selection criteria and by comparing the probability to prolong tracks from the TPC inward to the ITS ('matching efficiency') in data and simulations. The variation of the track selection criteria, such as the minimum number of clusters in the TPC, was found to yield a 2% systematic effect on the cross section of D^0 mesons (two-prong final state) and 3% for the other meson species (three-prong final states). The comparison of the matching efficiency in data and simulations was made after weighting the relative abundances of primary and secondary particles in the simulation to match those observed in data. This weighting is motivated by the observation that the matching efficiency is much larger for primary particles than for secondary particles produced far from the interaction point in decays of strange hadrons and in interactions of primary particles with the material of the detector. The fractions of primary and secondary particles were estimated, as a function of p_T, by fitting the inclusive track impact parameter distributions in data and in the simulation with a sum of three template distributions for primary particles, for secondary particles from strange-hadron decays and for secondary particles produced in interactions of primary particles in the detector material. The templates were obtained from the simulation. After weighting the relative abundances in the simulation to match those in data, the systematic uncertainty on the matching efficiency was defined as the relative difference of the matching efficiencies in data and in the simulation. The study was made separately for particles identified

Table 1 Summary of relative systematic uncertainties for two p_T intervals

p_T (GeV/c)	D^0		D^+		D^{*+}		D_s^+	
	2–3	10–12	2–3	10–12	2–3	10–12	2–4	8–12
Signal yield	3%	4%	6%	5%	2%	2%	5%	5%
Tracking efficiency	4%	4%	4%	6%	6%	6%	5%	6%
Selection efficiency	5%	5%	10%	5%	5%	5%	7%	7%
PID efficiency	0	0	0	0	0	0	7%	7%
p_T Shape in MC	0	0	1%	2%	2%	0	3%	2%
Feed-down	$^{+4}_{-4}$%	$^{+3}_{-5}$%	$^{+2}_{-3}$%	$^{+2}_{-3}$%	$^{+2}_{-2}$%	$^{+2}_{-3}$%	$^{+4}_{-5}$%	$^{+4}_{-5}$%
Branching ratio	1.0%		2.5%		1.3%		3.5%	
Normalisation	3.5%							

as pions and as kaons using the TPC and TOF PID selections described in Sect. 2. The systematic uncertainty is 2% per track in the interval $2 < p_T < 6$ GeV/c and 1% at lower and higher p_T. The per-track uncertainty was then propagated to the D mesons, taking into account the number and transverse momentum of their decay tracks, and added in quadrature to the component estimated from the track selection variation.

Systematic uncertainties can also arise from possible differences in the distributions and resolution of the geometric selection variables between data and the simulation. These uncertainties were evaluated by repeating the analysis with several sets of selection criteria and comparing the resulting corrected cross sections. More details can be found in [14].

To estimate the uncertainty on the PID selection efficiency, for the three non-strange D-meson species the analysis was repeated without PID selection. The resulting cross sections were found to be compatible with those obtained with the PID selection. Therefore, no systematic uncertainty was assigned. For the D_s^+ meson, the lower signal yield and the larger combinatorial background prevented a signal estimation without particle identification, hence, in this case, a 3σ PID selection, looser with respect to the PID strategy adopted in the analysis, was used to estimate a systematic uncertainty of about 7%.

The systematic effect on the efficiency due to a possible difference between the simulated and real p_T distribution of D mesons was estimated by using alternative D-meson p_T distributions from the PYTHIA 6 generator with Perugia-0 tune and from the FONLL pQCD calculation. More details can be found in [14].

The systematic uncertainty on the subtraction of feed-down from beauty-hadron decays includes the uncertainties of (i) the B-meson production cross section from FONLL calculations, (ii) the branching ratios of B mesons into D mesons [36] and (iii) the relative abundances of B-meson species produced in the beauty-quark fragmentation [36]. The dominant contribution is the one originating from the FONLL calculations and it was estimated by varying the p_T-differential

cross section of feed-down D mesons within the theoretical uncertainties of the FONLL calculation. The procedure for the variation of the b-quark mass, of the perturbative scales and of the parton distribution functions is described in [7]. In previous analyses, an alternative method based on the ratio of the FONLL cross sections for feed-down and prompt D mesons was also used in the estimation of the systematic uncertainties. In this analysis it was no longer used, on the basis of the observation that FONLL calculations at LHC energies provide a good description of the production cross sections of B^0, B^+ and B_s^0 mesons at both central and forward rapidity, while it underestimates prompt charm production [43–48]. Hence, the uncertainty due to the B feed-down correction is significantly reduced and more symmetric as compared to our previous publications.

The uncertainty on the D-meson production cross section normalisation has a contribution from the 3.5% uncertainty on the minimum-bias trigger cross section [37] and a contribution from the uncertainties on the branching ratios of the considered D-meson decay channels (see Table 1).

The total systematic uncertainties, which are obtained as a quadratic sum of the contributions listed in Table 1, are reduced by a factor that ranges from 1.5 to 5, depending on D-meson species and p_T interval, with respect to previous publications [14,16]. The systematic uncertainties on PID, tracking and selection efficiencies are mostly correlated among the different p_T intervals, while the raw-yield extraction uncertainty is mostly uncorrelated.

4 Results

The p_T-differential cross sections for prompt D^0, D^+, D^{*+} and D_s^+ production in $|y| < 0.5$ are shown in Fig. 3. The error bars represent the statistical uncertainties, while the systematic uncertainties are shown as boxes around the data points. The symbols are positioned horizontally at the centre of each p_T interval, with the horizontal bars representing the width of the p_T interval. For all D-meson species, the results
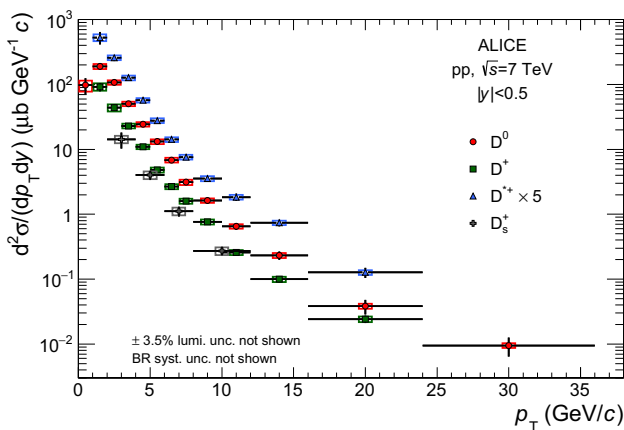
Fig. 3 p_T-differential inclusive production cross section of prompt D^0, D^+, D^{*+} and D_s^+ mesons in pp collisions at $\sqrt{s} = 7$ TeV. Statistical uncertainties (*bars*) and systematic uncertainties (*boxes*) are shown. The D^{*+} cross section is scaled by a factor of 5 for better visibility

are consistent within uncertainties with those reported in our previous publications on charmed-meson cross sections in pp collisions at $\sqrt{s} = 7$ TeV [14,16], but the total uncertainties (sum in quadrature of statistical and systematic errors) are reduced by a factor 1.5–4, depending on the D-meson species and the p_T interval. The D^0-meson cross section in the interval $0 < p_T < 1$ GeV/c is obtained from the analysis without decay vertex reconstruction described in Ref. [17]. At higher p_T, the results of the analysis presented in this paper, based on geometrical selections on the displaced decay vertex, are more precise than those obtained without decay vertex reconstruction.

In Figs. 4, 5, 6 and 7, the measured p_T-differential cross sections are compared with results from perturbative QCD calculations, two of which are based on collinear factorisation (FONLL [6,7] and GM-VFNS [3–5]) and one is a leading order (LO) calculation based on k_T-factorisation [9]. The results of these calculations, performed in the same p_T intervals of the measurement, are shown as filled boxes spanning the theoretical uncertainties and a solid line representing the values obtained with the central values of the pQCD parameters. The theoretical uncertainties are estimated in all the three frameworks by varying the renormalisation and factorisation scales. In the FONLL and k_T-factorisation calculations also the effect of the charm-quark mass uncertainty is considered. In the FONLL and GM-VFNS calculations, the CTEQ6.6 PDFs [49] were used, and the uncertainty on the PDFs was included in the FONLL error boxes. The LO k_T-factorisation calculations were performed with an updated set of unintegrated gluon-distribution functions computed from the recent MMHT2014-LO PDFs [50]. For this reason, the comparison to the measured D^0-meson cross section differs from that reported in Ref. [17]. In the FONLL calculation, the fragmentation fractions $f(c \rightarrow D)$, i.e. the fractions of

charm quarks hadronising into each D-meson species, were taken from Ref. [51]. For the D_s^+ mesons, only the comparisons to GM-VFNS and LO k_T-factorisation predictions are shown, because a calculation of the D_s^+ production cross section within the FONLL framework is not available. The central value of the GM-VFNS predictions lies systematically above the data, while that of the FONLL predictions lies below the data. For FONLL, this feature was observed also at other values of $\sqrt{s}$, from 0.2 to 13 TeV [11,12,15,19–21]. The LO k_T-factorisation calculation describes the data within uncertainties for $p_T < 2$ GeV/c and $p_T > 10$ GeV/c, while in the interval $2 < p_T < 10$ GeV/c the predictions underestimate the measured production cross sections.

The average transverse momentum $\langle p_T \rangle$ of prompt D^0 mesons was measured by fitting the cross section reported in Fig. 4 with a power-law function:

$$f(p_T) = C \frac{p_T}{(1 + (p_T/p_0)^2)^n},\tag{3}$$

where C, p_0 and n are the free parameters. The prompt-D^0 $\langle p_T \rangle$, defined as the mean value of the fit function, is:

$$\langle p_T \rangle_{\text{pp, 7 TeV}}^{\text{prompt }D^0} = 2.19 \pm 0.06 \,(\text{stat.}) \pm 0.04 \,(\text{syst.}) \,\text{GeV}/c.\tag{4}$$

The systematic uncertainty on $\langle p_T \rangle$ was estimated as described in Ref. [17] taking into account separately the contributions due to the correlated and uncorrelated systematic uncertainties on the measured p_T-differential cross section. The uncertainty due to the fit function was estimated from the spread of the results obtained with different functions and using an alternative method, which is not based on fits to the distribution, but on direct calculations of $\langle p_T \rangle$ from the data points.

The ratios of the p_T-differential cross sections of D^0, D^+, D^{*+} and D_s^+ mesons are reported in Fig. 8. In the evaluation of the systematic uncertainties on these ratios, the sources of correlated and uncorrelated systematic effects were treated separately. In particular, the contributions of the yield extraction and cut efficiency were considered as uncorrelated, while those of the feed-down from beauty-hadron decays and the tracking efficiency were treated as fully correlated among the different D-meson species. The measured D-meson ratios do not show a significant p_T dependence within the experimental uncertainties, thus suggesting a small difference between the fragmentation functions of charm quarks to pseudoscalar (D^0, D^+ and D_s^+) and vector (D^{*+}) mesons and to strange and non-strange mesons. The data are compared to the ratios of the D-meson cross sections from FONLL (only for D^0, D^+ and D^{*+} mesons), GM-VFNS and LO k_T-factorisation pQCD calculations. The ratios of the theoretical predictions were computed assuming their uncertainties to be fully correlated among the D-meson species, which results in an almost

Fig. 4 p_T-differential production cross section of prompt D^0 mesons with $|y| < 0.5$ in the interval $0 < p_T < 36$ GeV/c, in pp collisions at $\sqrt{s} = 7$ TeV. The data point in $0 < p_T < 1$ GeV/c is obtained from the analysis without decay vertex reconstruction described in Ref. [17]. The cross section is compared to three pQCD calculations: FONLL [7] (*top-left panel*), GM-VFNS [5] (*top-right panel*) and a leading order (LO) calculation based on k_T-factorisation [9] (*bottom panel*). The ratios of the data to the three calculated cross sections are shown in the *lower part of each panel*. In the data-to-theory ratios the 3.5% normalisation uncertainty due to the luminosity determination is not included in the systematic uncertainty on the data points
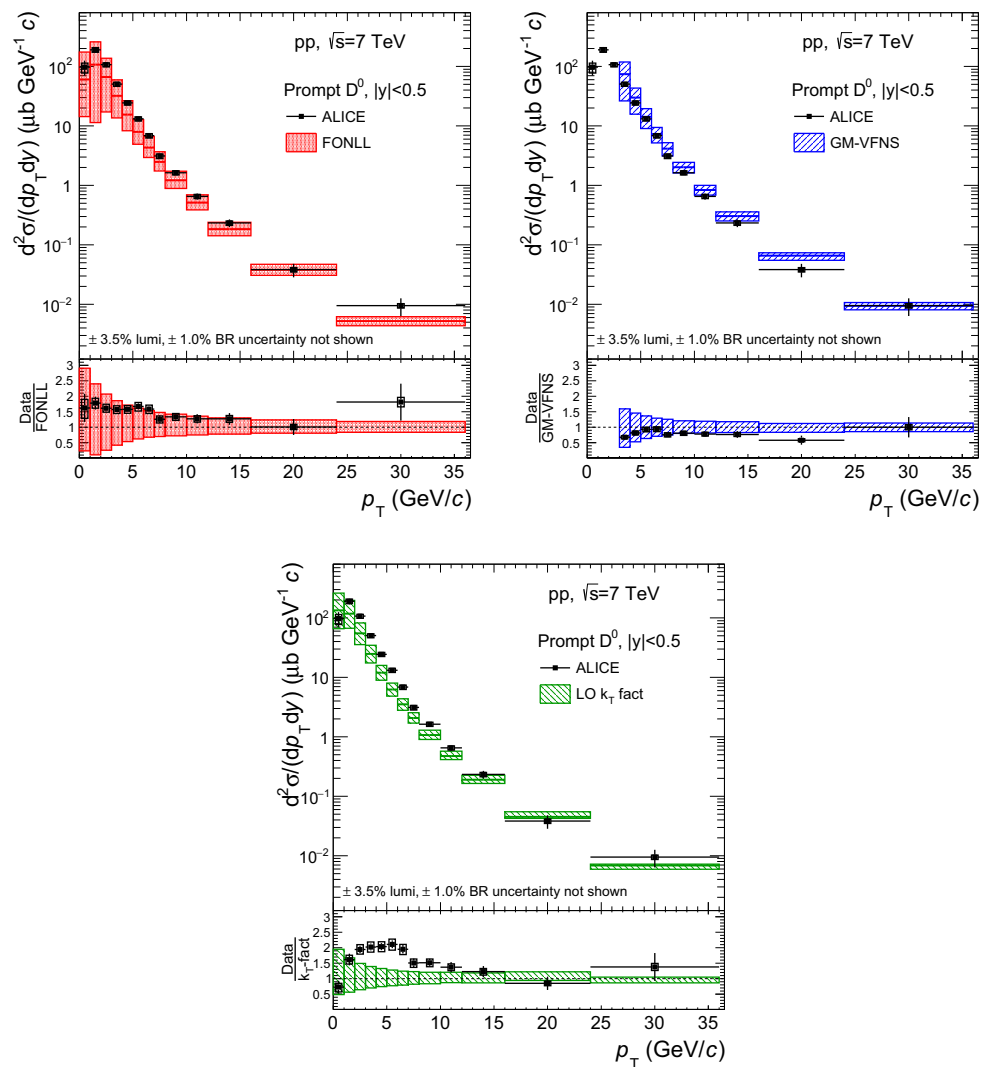
complete cancellation of the uncertainties in the ratio. Note that in all these pQCD calculations, the relative abundances of the different D-meson species are not predicted by the theory, but the fragmentation fractions, $f(c \to D)$, are taken from the experimental measurements [7,9,51–54]. In the FONLL and GM-VFNS frameworks, the p_T dependence of the ratios of the D-meson production cross sections arises from the different fragmentation functions used to model the transfer of energy from the charm quark to a specific D-meson species [52,53,55], and from the different contribution from decays of higher excited states. The parton fragmentation models used in the calculations provide an adequate description of the measured data. In the LO k_T-factorisation calculations, the same fragmentation function (Peterson [56]) is used for D^0, D^+ and D_s^+ mesons, resulting in the same shape of the p_T distributions of these three meson species, while the fragmentation functions for vector mesons from Ref. [57] are used for D^{*+} mesons [9].

The ratios of D^0-meson production cross sections in different rapidity intervals, which are expected to be sensitive to the gluon PDF at small values of Bjorken-x [22], were computed from our measurement in the central rapidity region ($|y| < 0.5$) and the results reported by the LHCb collaboration for pp collisions at $\sqrt{s} = 7$ TeV in different y intervals at forward rapidity [19]. The results are reported in Fig. 9, where the central-to-forward ratios are shown as a function of p_T for three different y intervals at forward rapidity: $2 < y < 2.5$ (left panel), $3 < y < 3.5$ (middle panel), $4 < y < 4.5$ (right panel). The error bars represent the total uncertainty obtained from the propagation of the statistical and systematic uncertainties on the p_T-differential cross sections. The measured ratios are compared to FONLL calculations, shown as boxes in Fig. 9. The central-to-forward ratios computed using the central values of the factorisation and renormalisation scales are found to describe the data within their uncertainties. The upper edge of the FONLL uncertainty band, which is also in agreement with the mea-

Fig. 5 p_T-differential production cross section of prompt D^+ mesons with $|y| < 0.5$ in the interval $1 < p_T < 24$ GeV/c, in pp collisions at $\sqrt{s} = 7$ TeV. The cross section is compared to three pQCD calculations: FONLL [7] (*top-left panel*), GM-VFNS [5] (*top-right panel*) and a leading order (LO) calculation based on k_T-factorisation [9] (*bottom panel*). The ratios of the data to the three calculated cross sections are shown in the *lower part of each panel*. In the data-to-theory ratios the 3.5% normalisation uncertainty due to the luminosity determination is not included in the systematic uncertainty on the data points
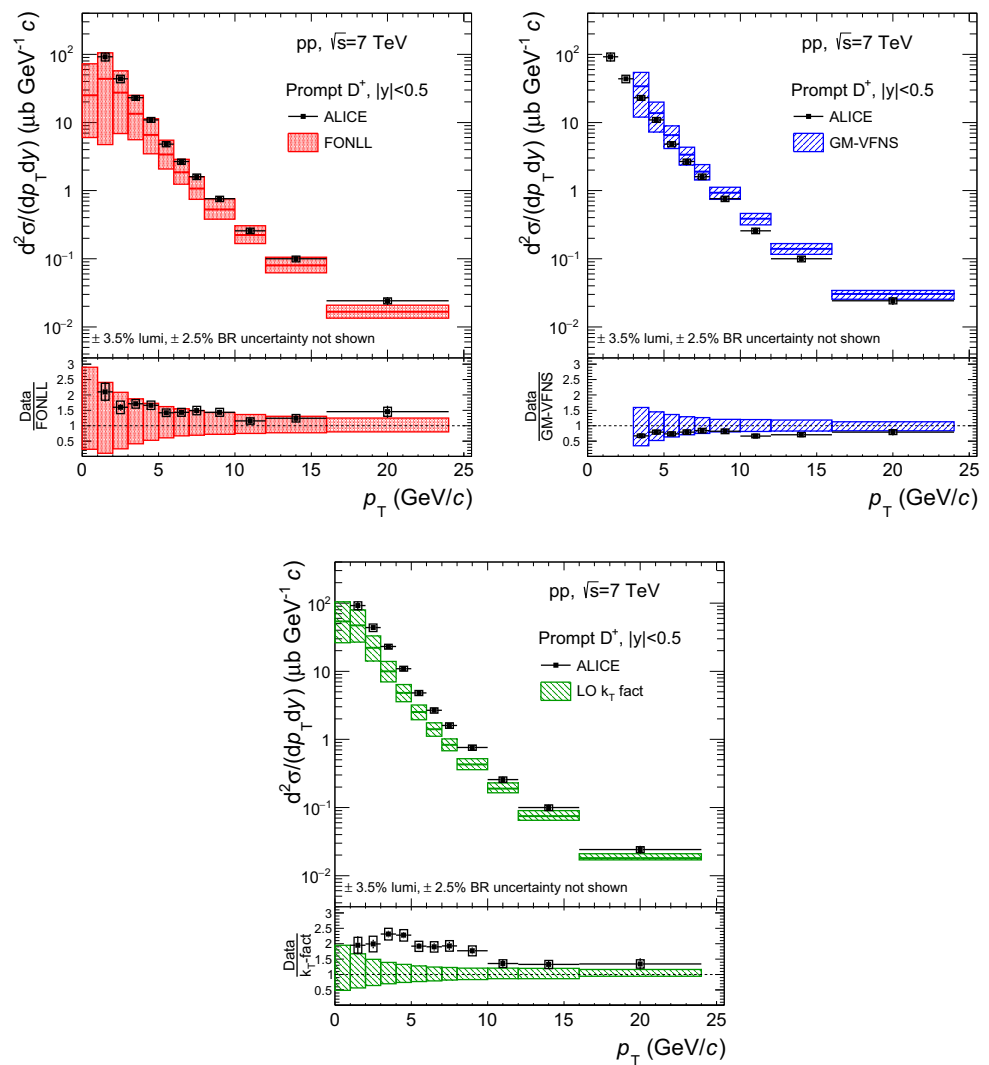
sured values of the central-to-forward ratios, is determined by the calculations with factorisation scale $\mu_F = 2 m_T$, where $m_T = \sqrt{p_T^2 + m_c^2}$ and $m_c = 1.5$ GeV/c^2. The low edge of the FONLL uncertainty band is determined by the calculations with $\mu_F = 0.5 m_T$, which provide a worse description of the measured central-to-forward ratios at low p_T for the most forward rapidity interval. Note that in this forward rapidity interval, the FONLL calculation with $\mu_F = 0.5 m_T$ uses the PDFs for Bjorken-x values reaching down to about 10^{-5}, a region that is not constrained by experimental data, and below $Q^2 = (1.3$ GeV/$c)^2$, where the CTEQ6.6 PDFs [49] are kept constant to their values at $(1.3$ GeV/$c)^2$.

The visible cross sections of prompt D mesons, obtained by integrating the p_T-differential cross sections in the measured p_T range, are reported in Table 2. In addition, for D^0 mesons the cross sections integrated over the p_T intervals of the D^+, D^{*+} and D_s^+ measurements are shown. The systematic uncertainty was defined by propagating the yield extraction uncertainties as uncorrelated among p_T intervals and all

the other uncertainties as correlated. These values were used to compute the ratios of the p_T-integrated D-meson production cross sections, which are reported in Table 3. The systematic uncertainties on the ratios were computed taking into account the sources correlated and uncorrelated among the different D-meson species as described above. The measured ratios are compatible within uncertainties with the results at $\sqrt{s} = 2.76$ TeV [15] and with the measurements of the LHCb collaboration at forward rapidity ($2.0 < y < 4.5$) at three different collision energies $\sqrt{s} = 5$, 7 and 13 TeV [19–21]. The measured p_T-integrated production ratios are also compatible with the charm-quark fragmentation fractions $f(c \rightarrow D)$ measured in e^+e^- collisions from the compilation in [51]. These results indicate that the fragmentation fractions of charm quarks into different D-meson species do not vary substantially with rapidity, collision energy and colliding system.

The production cross sections per unit of rapidity, $d\sigma/dy$, at mid-rapidity were computed for each meson species by

Fig. 6 p_T-differential production cross section of prompt D^{*+} mesons with $|y| < 0.5$ in the interval $1 < p_T < 24$ GeV/c, in pp collisions at $\sqrt{s} = 7$ TeV. The cross section is compared to three pQCD calculations: FONLL [7] (*top-left panel*), GM-VFNS [5] (*top-right panel*) and a leading order (LO) calculation based on k_T-factorisation [9] (*bottom panel*). The ratios of the data to the three calculated cross sections are shown in the lower part of each panel. In the data-to-theory ratios the 3.5% normalisation uncertainty due to the luminosity determination is not included in the systematic uncertainty on the data points
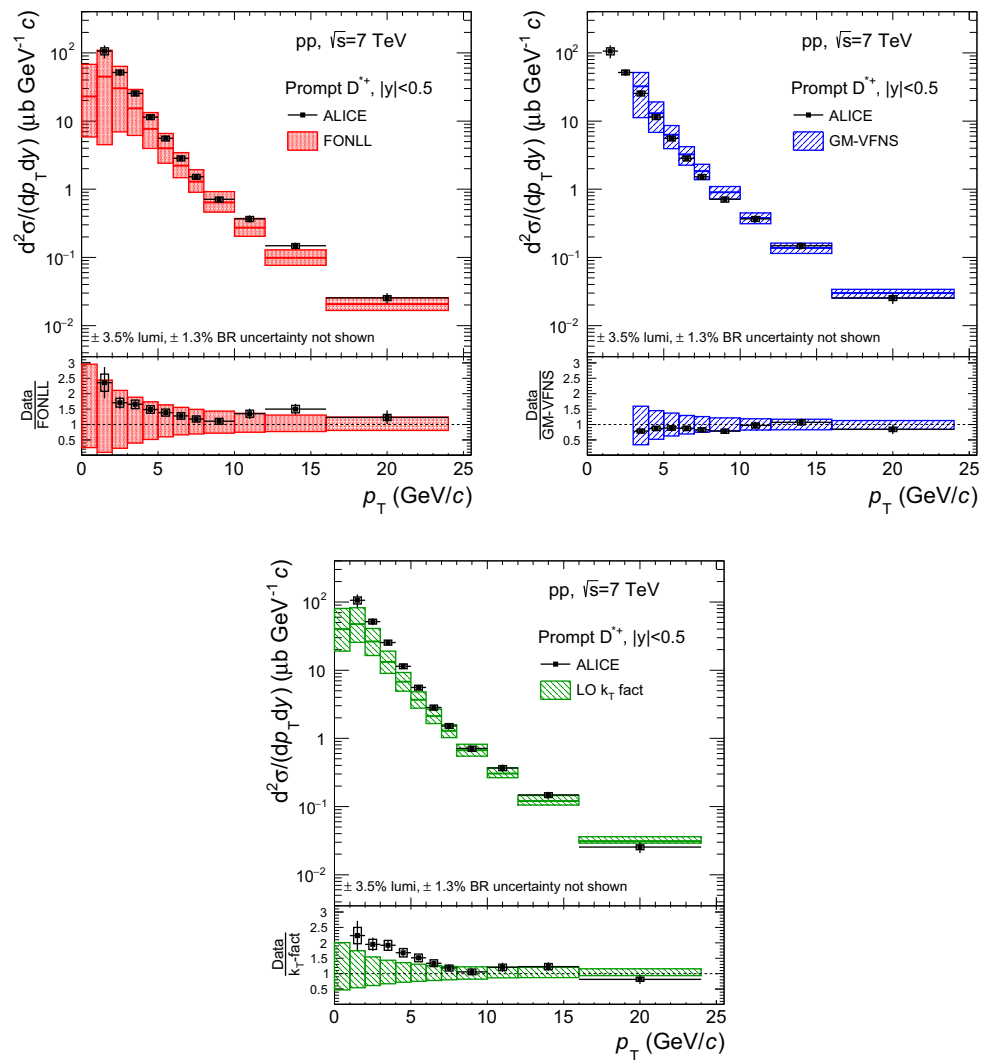

Fig. 7 p_T-differential production cross section of prompt D$_s^+$ mesons with $|y| < 0.5$ in the interval $2 < p_T < 12$ GeV/c, in pp collisions at $\sqrt{s} = 7$ TeV. The cross section is compared to two pQCD calculations: GM-VFNS [5] (*left panel*) and a leading order (LO) calculation based on k_T-factorisation [9] (*right panel*). The ratios of the data to the calculated cross sections are shown in the lower part of each panel. In the data-to-theory ratios the 3.5% normalisation uncertainty due to the luminosity determination is not included in the systematic uncertainty on the data points
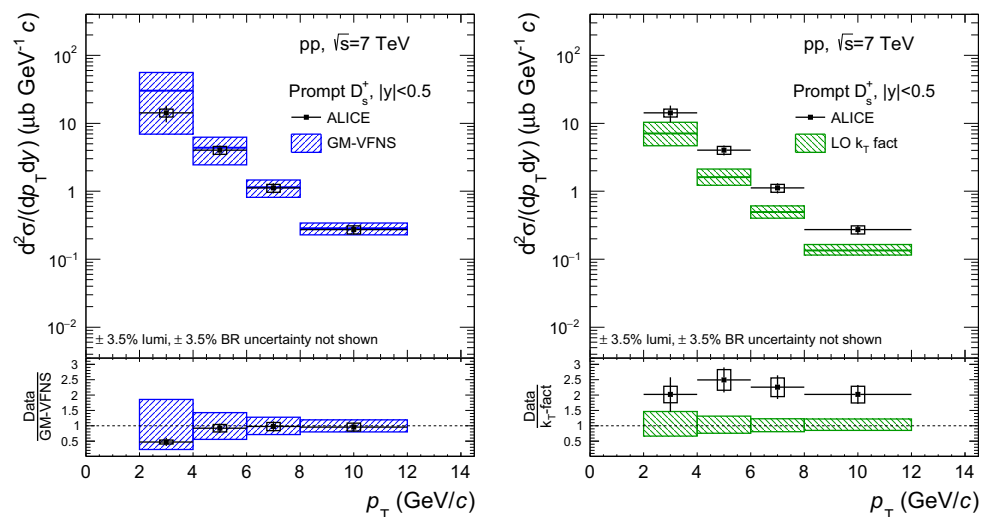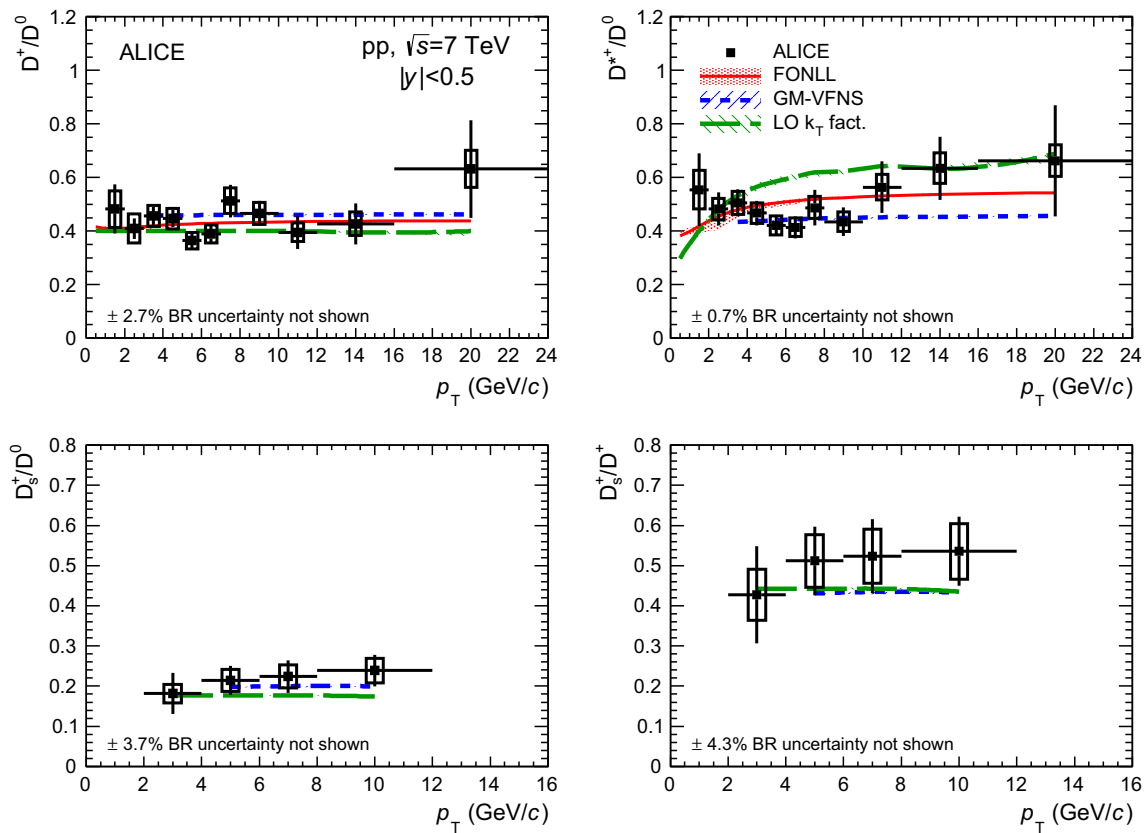
Fig. 8 Ratios of D-meson production cross sections as a function of p_T. Predictions from FONLL, GM-VFNS and LO k_T-factorisation calculations are also shown. For the pQCD calculations the *line* shows the ratio of the central values of the theoretical cross sections, while the *shaded area* is defined by the ratios computed from the upper and lower limits of the theoretical uncertainty band
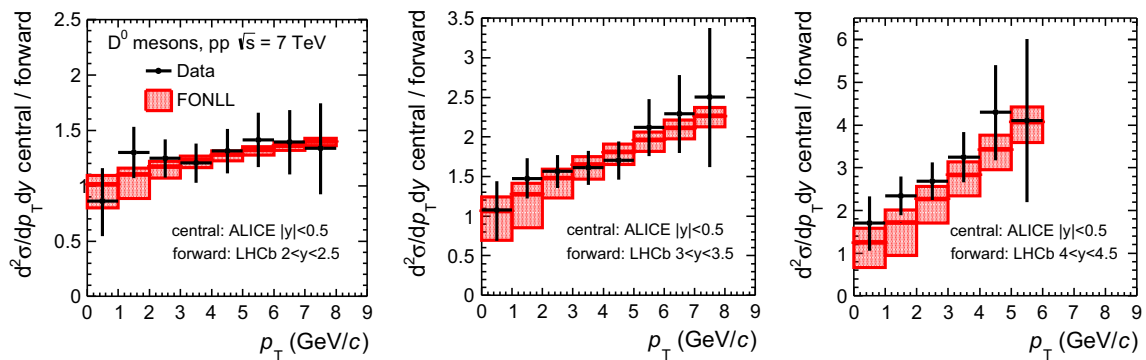

Fig. 9 Ratios of D^0-meson production cross section per unit of rapidity at mid-rapidity ($|y| < 0.5$) to that measured by the LHCb Collaboration [19] in three rapidity ranges, $2 < y < 2.5$ (*left panel*), $3 < y < 3.5$ (*middle panel*), $4 < y < 4.5$ (*right panel*), as a function of p_T. The LHCb measurement were multiplied by 2 to refer them to one unit of rapidity. The *error bars* represent the total (statistical and systematic) uncertainty on the measurement. Predictions from FONLL calculations are compared to the data points

extrapolating the visible cross section to the full p_T range. The extrapolation factor for a given D-meson species was defined as the ratio between the total production cross section in $|y| < 0.5$ and that in the experimentally covered phase space, both of them calculated with the FONLL central

parameters. The systematic uncertainty on the extrapolation factor was estimated by considering the contributions due to (i) the uncertainties on the CTEQ6.6 PDFs [49] and (ii) the variation of the charm-quark mass and the renormalisation and factorisation scales in the FONLL calculation, as pro-

Table 2 Visible production cross sections of prompt D mesons in $|y| < 0.5$ in pp collisions at $\sqrt{s} = 7$ TeV

	Kinematic range	Visible cross section (μb)
D^0	$0 < p_T < 36$ GeV/c	$500 \pm 36\text{(stat)} \pm 39\text{(syst)} \pm 18\text{(lumi)} \pm 5\text{(BR)}$
	$1 < p_T < 24$ GeV/c	$402 \pm 24\text{(stat)} \pm 28\text{(syst)} \pm 14\text{(lumi)} \pm 4\text{(BR)}$
	$2 < p_T < 12$ GeV/c	$210 \pm 7\text{(stat)} \pm 14\text{(syst)} \pm 7\text{(lumi)} \pm 2\text{(BR)}$
D^+	$1 < p_T < 24$ GeV/c	$182 \pm 14\text{(stat)} \pm 20\text{(syst)} \pm 6\text{(lumi)} \pm 5\text{(BR)}$
	$2 < p_T < 12$ GeV/c	$89 \pm 3\text{(stat)} \pm 9\text{(syst)} \pm 3\text{(lumi)} \pm 2\text{(BR)}$
D^{*+}	$1 < p_T < 24$ GeV/c	$207 \pm 24\text{(stat)} \pm 20\text{(syst)} \pm 7\text{(lumi)} \pm 3\text{(BR)}$
	$2 < p_T < 12$ GeV/c	$101 \pm 6\text{(stat)} \pm 8\text{(syst)} \pm 4\text{(lumi)} \pm 1\text{(BR)}$
D_s^+	$2 < p_T < 12$ GeV/c	$40 \pm 8\text{(stat)} \pm 5\text{(syst)} \pm 1\text{(lumi)} \pm 1\text{(BR)}$

Table 3 Ratios of the measured p_T-integrated cross sections of prompt D mesons in $|y| < 0.5$ in pp collisions at $\sqrt{s} = 7$ TeV

	Kinematic range	Production cross section ratio
$\sigma(D^+)/\sigma(D^0)$	$1 < p_T < 24$ GeV/c	$0.45 \pm 0.04\text{(stat)} \pm 0.05\text{(syst)} \pm 0.01\text{(BR)}$
$\sigma(D^{*+})/\sigma(D^0)$	$1 < p_T < 24$ GeV/c	$0.52 \pm 0.07\text{(stat)} \pm 0.05\text{(syst)} \pm 0.01\text{(BR)}$
$\sigma(D_s^+)/\sigma(D^0)$	$2 < p_T < 12$ GeV/c	$0.19 \pm 0.04\text{(stat)} \pm 0.02\text{(syst)} \pm 0.01\text{(BR)}$
$\sigma(D_s^+)/\sigma(D^+)$	$2 < p_T < 12$ GeV/c	$0.45 \pm 0.09\text{(stat)} \pm 0.06\text{(syst)} \pm 0.02\text{(BR)}$

Table 4 Production cross sections of prompt D mesons in $|y| < 0.5$ and full p_T range in pp collisions at $\sqrt{s} = 7$ TeV

	Extr. factor to $p_T > 0$	$d\sigma/dy\,|_{|y|<0.5}$ (μb)
D^0	$1.0002^{+0.0004}_{-0.0002}$	$500 \pm 36\text{(stat)} \pm 39\text{(syst)} \pm 18\text{(lumi)} \pm 5\text{(BR)}$
D^+	$1.25^{+0.29}_{-0.09}$	$227 \pm 18\text{(stat)} \pm 25\text{(syst)} \pm 8\text{(lumi)} \pm 6\text{(BR)}^{+52}_{-16}\text{(extrap)}$
D^{*+}	$1.21^{+0.28}_{-0.08}$	$251 \pm 29\text{(stat)} \pm 24\text{(syst)} \pm 9\text{(lumi)} \pm 3\text{(BR)}^{+58}_{-16}\text{(extrap)}$
D_s^+	$2.23^{+0.71}_{-0.65}$	$89 \pm 18\text{(stat)} \pm 11\text{(syst)} \pm 3\text{(lumi)} \pm 3\text{(BR)}^{+28}_{-26}\text{(extrap)}$

posed in [7]. For D^0 mesons, which are measured down to $p_T = 0$, the extrapolation factor accounts only for the very small contribution of D-mesons with $p_T > 36$ GeV/c and it has therefore a value very close to unity with negligible uncertainty. In the case of D_s^+ mesons, for which a FONLL prediction is not available, the central value of the extrapolation factor was computed from the prediction based on the p_T-differential cross section of charm quarks from FONLL, the fractions $f(c \to D_s^+)$ and $f(c \to D_s^{*+})$ from ALEPH [54], and the fragmentation functions from [57], which have one parameter, r, that was set to 0.1 as done in FONLL [53]. The D_s^{*+} mesons produced in the c quark fragmentation were made to decay with PYTHIA and the resulting D_s^+ mesons were summed to the primary ones to obtain the prompt yield. An additional contribution to the systematic uncertainty was assigned for D_s^+ mesons based on the envelope of the results obtained using the FONLL p_T-differential cross sections of D^0, D^+ and D^{*+} mesons to compute the D_s^+ extrapolation factor. The resulting values for the extrapolation factors and for the prompt D-meson production cross sections per unit of rapidity $d\sigma/dy$ are reported in Table 4.

The $c\bar{c}$ production cross section per unit of rapidity at mid-rapidity ($|y| < 0.5$) was calculated by dividing the prompt D^0-meson cross section by the fraction of charm quarks hadronising into D^0 mesons $f(c \to D^0)$ and correct-

ing for the different shapes of the distributions of y_{D^0} and $y_{c\bar{c}}$ ($c\bar{c}$ pair rapidity). The correction factor and its uncertainty were extracted from FONLL and MNR NLO pQCD [58] calculations together with PYTHIA 6 [38] and POWHEG [59] simulations, as described in detail in Ref. [17]. For the fragmentation fraction, the value $f(c \to D^0) = 0.542 \pm 0.024$ derived in Ref. [51] by averaging the measurements from e^+e^- collisions at LEP was used. As pointed out in Refs. [60,61], measurements in e^+e^-, ep and pp collisions agree within uncertainties, supporting the hypothesis that fragmentation is independent of the specific production process.[1] The resulting $c\bar{c}$ cross section per unit of rapidity at mid-rapidity is:

$$d\sigma^{c\bar{c}}_{\text{pp, 7 TeV}}/dy \Big|_{|y|<0.5} = 954 \pm 69\,\text{(stat)} \pm 74\,\text{(syst)}$$
$$\pm 33\,\text{(lumi)} \pm 42\,\text{(FF)} \pm 31\,\text{(rap.shape)}\;\mu\text{b}. \tag{5}$$

We verified that the precision of the $c\bar{c}$ production cross-section determination does not improve if the results calculated from D^+, D^{*+} and D_s^+ mesons, which have significantly

---

[1] In Ref. [61], an average of the charm fragmentation fractions over the measurements from all collision systems is calculated, imposing the constraint that the sum of all weakly-decaying charmed hadrons is unity, which results in $f(c \to D^0) = 0.6086 \pm 0.0076$ (about 11% larger that the value from [51]).

larger extrapolation uncertainties as compared to the D^0 one, are included via a weighted average procedure, as done in Ref. [15]. The total production cross section of prompt D^0 mesons (average of particles and antiparticles) was calculated by extrapolating to full phase space the cross section measured at mid-rapidity. The extrapolation factor was defined as the ratio of the D^0 production cross sections in full rapidity and in $|y| < 0.5$ calculated with the FONLL central parameters: $8.56^{+2.51}_{-0.42}$. The systematic uncertainty on the extrapolation factor was estimated with the same procedure described above for the p_T extrapolation. The resulting cross section is:

$$\sigma^{\text{prompt } D^0}_{\text{pp, 7 TeV}} = 4.28 \pm 0.31 \,(\text{stat}) \pm 0.33 \,(\text{syst}) \,^{+1.26}_{-0.24} \,(\text{extr.})$$
$$\pm 0.15 \,(\text{lumi}) \pm 0.04 \,(\text{BR}) \text{ mb}. \tag{6}$$

The total charm production cross section was calculated by dividing the total prompt D^0-meson production cross section by the fragmentation fraction reported above. The resulting $c\bar{c}$ production cross section in pp collisions at $\sqrt{s} = 7$ TeV is:

$$\sigma^{c\bar{c}}_{\text{pp, 7 TeV}}(\text{ALICE}) = 7.89 \pm 0.57 \,(\text{stat.})$$
$$\pm 0.61 \,(\text{syst.}) \,^{+2.32}_{-0.45}(\text{extr.}) \pm 0.28 \,(\text{lumi.}) \pm 0.35 \,(\text{FF}) \text{ mb}, \tag{7}$$

which is consistent with the value of Ref. [17] but has smaller statistical and systematic uncertainties. It is also compatible within uncertainties with the total charm production cross section reported by the ATLAS collaboration [13], which is calculated from D^+ and D^{*+} measurements in $|\eta| < 2.1$ and $p_T > 3.5$ GeV/c and has larger uncertainties on the extrapolation to full kinematic phase space as compared to our result.

A more precise determination of the $c\bar{c}$ production cross section can be obtained by summing our measurement of the prompt D^0-meson cross section in $|y| < 0.5$ and the LHCb result in $2 < y < 4.5$ for $0 < p_T < 8$ GeV/c [19], and extrapolating to full rapidity and p_T via the ratio of FONLL calculations of the cross sections in full phase space and in the measured y and p_T intervals exploiting the symmetry around $y = 0$. The result for the $c\bar{c}$ production cross section is:

$$\sigma^{c\bar{c}}_{\text{pp, 7 TeV}}(\text{ALICE, LHCb}) = 7.44 \pm 0.14 \,(\text{stat.})$$
$$\pm 0.46 \,(\text{syst.}) \,^{+0.13}_{-0.07}(\text{extr.}) \pm 0.33 \,(\text{FF}) \text{ mb}, \tag{8}$$

where the +0.13 mb extrapolation uncertainty is determined by FONLL calculations with factorisation scale $\mu_F = 0.5\,m_T$, which do not describe the measured central-to-forward ratios of Fig. 9. If this μ_F value is not considered, the extrapolation uncertainty is reduced to ± 0.07 mb.

5 Summary

We have presented a new measurement of the inclusive p_T-differential production cross sections of prompt D^0, D^+, D^{*+} and D^+_s mesons at mid-rapidity ($|y| < 0.5$) in pp collisions at a centre-of-mass energy of $\sqrt{s} = 7$ TeV. The measurements cover the transverse-momentum interval $0 < p_T < 36$ GeV/c for D^0 mesons, $1 < p_T < 24$ GeV/c for D^+ and D^{*+} mesons, and $2 < p_T < 12$ GeV/c for D^+_s mesons. As compared to previously published results based on the same data sample [14,16], the present results have an extended p_T coverage and total uncertainties reduced by a factor of about 1.5–4 depending on the D-meson species and p_T. The measurements cover complementary ranges in p_T and y with respect to those of the ATLAS ($3.5 < p_T < 100$ GeV/c, $|\eta| < 2.1$ [13]) and LHCb ($0 < p_T < 8$ GeV/c, $2 < y < 4.5$ [19]) Collaborations at the same centre-of-mass energy. The p_T-differential cross sections are described within uncertainties in the full p_T range by the FONLL and GM-VFNS perturbative QCD calculations, which are based on collinear factorisation, while a leading-order calculation based on k_T factorisation underestimates the measured cross sections for $2 < p_T < 10$ GeV/c. The p_T-differential ratios of our measurement at mid-rapidity and LHCb measurements at forward rapidity [19] are described by FONLL calculations. These central-to-forward ratios, once complemented with similar measurements at different centre-of-mass energies, could provide sensitivity to the gluon PDF at small values of Bjorken-x [22]. The ratios of the cross sections of the four D-meson species were found to be compatible with the LHCb measurements at forward rapidity and different collision energies as well as with results from e^+e^- collisions, indicating that the fragmentation fractions of charm quarks into different D-meson species do not vary substantially with rapidity, collision energy and colliding system.

The new measurement also allowed for a more accurate determination of the p_T-integrated $c\bar{c}$ production cross section at mid-rapidity in pp collisions at $\sqrt{s} = 7$ TeV:

$$d\sigma^{c\bar{c}}_{\text{pp, 7 TeV}}/dy \Big|_{|y|<0.5} = 954 \pm 69 \,(\text{stat}) \pm 97 \,(\text{tot. syst.}) \,\mu\text{b}.$$

In particular, the total systematic uncertainty of this measurement is about $\pm 10\%$, while it was $^{+13}_{-21}\%$ for the previously-published measurement [17].

The total $c\bar{c}$ production cross section in full phase space was calculated by combining the above measurement at mid-rapidity with that at forward rapidity by the LHCb Collaboration:

$$\sigma^{c\bar{c}}_{\text{pp, 7 TeV}}(\text{ALICE, LHCb}) = 7.44 \pm 0.14 \,(\text{stat.})$$
$$\pm 0.58 \,(\text{tot. syst.}) \text{ mb}.$$

References

1. J.C. Collins, D.E. Soper, G.F. Sterman, Factorization of hard processes in QCD. Adv. Ser. Direct. High Energy Phys. **5**, 1–91 (1989). arXiv:hep-ph/0409313 [hep-ph]
2. S. Catani, M. Ciafaloni, F. Hautmann, High-energy factorization and small x heavy flavor production. Nucl. Phys. B **366**, 135–188 (1991)
3. B.A. Kniehl, G. Kramer, I. Schienbein, H. Spiesberger, Inclusive D*+- production in p anti-p collisions with massive charm quarks. Phys. Rev. D **71**, 014018 (2005). arXiv:hep-ph/0410289 [hep-ph]
4. B.A. Kniehl, G. Kramer, I. Schienbein, H. Spiesberger, Collinear subtractions in hadroproduction of heavy quarks. Eur. Phys. J. C **41**, 199–212 (2005). arXiv:hep-ph/0502194 [hep-ph]
5. B.A. Kniehl, G. Kramer, I. Schienbein, H. Spiesberger, Inclusive charmed-meson production at the CERN LHC. Eur. Phys. J. C **72**, 2082 (2012). arXiv:1202.0439 [hep-ph]
6. M. Cacciari, M. Greco, P. Nason, The p_T spectrum in heavy flavor hadroproduction. JHEP **05**, 007 (1998). arXiv:hep-ph/9803400 [hep-ph]
7. M. Cacciari, S. Frixione, N. Houdeau, M.L. Mangano, P. Nason, G. Ridolfi, Theoretical predictions for charm and bottom production at the LHC. JHEP **10**, 137 (2012). arXiv:1205.6344 [hep-ph]
8. M. Luszczak, R. Maciula, A. Szczurek, Nonphotonic electrons at RHIC within k(t)-factorization approach and with experimental semileptonic decay functions. Phys. Rev. D **79**, 034009 (2009). arXiv:0807.5044 [hep-ph]
9. R. Maciula, A. Szczurek, Open charm production at the LHC—k_t-factorization approach. Phys. Rev. D **87**(9), 094022 (2013). arXiv:1301.3033 [hep-ph]
10. A. Andronic et al., Heavy-flavour and quarkonium production in the LHC era: from proton-proton to heavy-ion collisions. Eur. Phys. J. C **76**(3), 107 (2016). arXiv:1506.03981 [nucl-ex]
11. STAR Collaboration, L. Adamczyk et al., Measurements of D^0 and D^{*+} production in pp collisions at $\sqrt{s} = 200$ GeV. Phys. Rev. D **86**, 072013 (2012). arXiv:1204.4244 [nucl-ex]
12. CDF Collaboration, D. Acosta et al., Measurement of prompt charm meson production cross sections in $p\bar{p}$ collisions at $\sqrt{s}$ = 1.96 TeV. Phys. Rev. Lett. **91**, 241804 (2003). arXiv:hep-ex/0307080 [hep-ex]
13. ATLAS Collaboration, G. Aad et al., Measurement of $D^{*\pm}$, $D^{\pm}$ and $D_s^{\pm}$ meson production cross sections in pp collisions at $\sqrt{s} = 7$ TeV with the ATLAS detector. Nucl. Phys. B **907**, 717–763 (2016). arXiv:1512.02913 [hep-ex]
14. ALICE Collaboration, B. Abelev et al., Measurement of charm production at central rapidity in proton–proton collisions at $\sqrt{s} = 7$ TeV. JHEP **01**, 128 (2012). arXiv:1111.1553 [hep-ex]
15. ALICE Collaboration, B. Abelev et al., Measurement of charm production at central rapidity in proton–proton collisions at $\sqrt{s} = 2.76$ TeV. JHEP **07**, 191 (2012). arXiv:1205.4007 [hep-ex]

16. ALICE Collaboration, B. Abelev et al., D_s^+ meson production at central rapidity in proton–proton collisions at $\sqrt{s} = 7$ TeV. Phys. Lett. B **718**, 279–294 (2012). arXiv:1208.1948 [hep-ex]

17. ALICE Collaboration, J. Adam et al., D-meson production in p-Pb collisions at $\sqrt{s_{NN}} = 5.02$ TeV and in pp collisions at $\sqrt{s} = 7$ TeV. Phys. Rev. C **94**(5), 054908 (2016). arXiv:1605.07569 [nucl-ex]

18. CMS Collaboration, D^0 meson nuclear modification factor in PbPb collisions at $\sqrt{s_{NN}} = 5.02$ TeV. Technical report. CMS-PAS-HIN-16-001, CERN, Geneva (2016). http://cds.cern.ch/record/2157844

19. LHCb Collaboration, R. Aaij et al., Prompt charm production in pp collisions at $\sqrt{s} = 7$ TeV. Nucl. Phys. B **871**, 1–20 (2013). arXiv:1302.2864 [hep-ex]

20. LHCb Collaboration, R. Aaij et al., Measurements of prompt charm production cross-sections in *pp* collisions at $\sqrt{s} = 5$ TeV. JHEP **06**, 147 (2017). doi:10.1007/JHEP06(2017)147 arXiv:1610.02230 [hep-ex]

21. LHCb Collaboration, R. Aaij et al., Measurements of prompt charm production cross-sections in *pp* collisions at $\sqrt{s} = 13$ TeV. JHEP **03**, 159 (2016), arXiv:1510.01707 [hep-ex] [Erratum: JHEP **09**, 013 (2016)]

22. M. Cacciari, M.L. Mangano, P. Nason, Gluon PDF constraints from the ratio of forward heavy-quark production at the LHC at $\sqrt{S} = 7$ and 13 TeV. Eur. Phys. J. C **75**(12), 610 (2015). arXiv:1507.06197 [hep-ph]

23. A. Bhattacharya, R. Enberg, M.H. Reno, I. Sarcevic, A. Stasto, Perturbative charm production and the prompt atmospheric neutrino flux in light of RHIC and LHC. JHEP **06**, 110 (2015). arXiv:1502.01076 [hep-ph]

24. A. Bhattacharya, R. Enberg, Y.S. Jeong, C.S. Kim, M.H. Reno, I. Sarcevic, A. Stasto, Prompt atmospheric neutrino fluxes: perturbative QCD models and nuclear effects. JHEP **11**, 167 (2016). arXiv:1607.00193 [hep-ph]

25. R. Gauld, J. Rojo, L. Rottoli, J. Talbert, Charm production in the forward region: constraints on the small-x gluon and backgrounds for neutrino astronomy. JHEP **11**, 009 (2015). arXiv:1506.08025 [hep-ph]

26. M.V. Garzelli, S. Moch, G. Sigl, Lepton fluxes from atmospheric charm revisited. JHEP **10**, 115 (2015). arXiv:1507.01570 [hep-ph]

27. F. Prino, R. Rapp, Open heavy flavor in QCD matter and in nuclear collisions. J. Phys. G **43**(9), 093002 (2016). arXiv:1603.00529 [nucl-ex]

28. A. Andronic, P. Braun-Munzinger, K. Redlich, J. Stachel, The thermal model on the verge of the ultimate test: particle production in Pb–Pb collisions at the LHC. J. Phys. G **38**, 124081 (2011). arXiv:1106.6321 [nucl-th]

29. X. Zhao, R. Rapp, Medium modifications and production of charmonia at LHC. Nucl. Phys. A **859**, 114–125 (2011). arXiv:1102.2194 [hep-ph]

30. Y.-P. Liu, Z. Qu, N. Xu, P.-F. Zhuang, J/ψ transverse momentum distribution in high energy nuclear collisions at RHIC. Phys. Lett. B **678**, 72–76 (2009). arXiv:0901.2757 [nucl-th]

31. ALICE Collaboration, B.B. Abelev et al., Centrality, rapidity and transverse momentum dependence of J/ψ suppression in Pb–Pb collisions at $\sqrt{s_{NN}} = 2.76$ TeV. Phys. Lett. B **734**, 314–327 (2014). arXiv:1311.0214 [nucl-ex]

32. ALICE Collaboration, J. Adam et al., Differential studies of inclusive J/ψ and $\psi(2S)$ production at forward rapidity in Pb–Pb collisions at $\sqrt{s_{NN}} = 2.76$ TeV. JHEP **05**, 179 (2016). arXiv:1506.08804 [nucl-ex]

33. ALICE Collaboration, K. Aamodt et al., The ALICE experiment at the CERN LHC. JINST **3**, S08002 (2008)

34. ALICE Collaboration, B.B. Abelev et al., Performance of the ALICE experiment at the CERN LHC. Int. J. Mod. Phys. A **29**, 1430044 (2014). arXiv:1402.4476 [nucl-ex]

35. ALICE Collaboration, J. Adam et al., Determination of the event collision time with the ALICE detector at the LHC. Eur. Phys. J. Plus **132**(2), 99 (2017). arXiv:1610.03055 [physics.ins-det]

36. C. Patrignani et al., Review of particle physics. Chin. Phys. C **40**(10), 100001 (2016)

37. ALICE Collaboration, B. Abelev et al., Measurement of inelastic, single- and double-diffraction cross sections in proton–proton collisions at the LHC with ALICE. Eur. Phys. J. C **73**(6), 2456 (2013). arXiv:1208.4968 [hep-ex]

38. T. Sjostrand, S. Mrenna, P.Z. Skands, PYTHIA 6.4 physics and manual. JHEP **05**, 026 (2006). arXiv:hep-ph/0603175 [hep-ph]

39. P.Z. Skands, Tuning Monte Carlo generators: the Perugia tunes. Phys. Rev. D **82**, 074018 (2010). arXiv:1005.3457 [hep-ph]

40. R. Brun, F. Bruyant, F. Carminati, S. Giani, M. Maire, A. McPherson, G. Patrick, L. Urban, GEANT detector description and simulation tool. Technical report. CERN (1994). http://cds.cern.ch/record/1082634

41. M. Cacciari, S. Frixione, P. Nason, The p(T) spectrum in heavy flavor photoproduction. JHEP **03**, 006 (2001). arXiv:hep-ph/0102134 [hep-ph]

42. D.J. Lange, The EvtGen particle decay simulation package. Nucl. Instrum. Methods A **462**, 152–155 (2001)

43. LHCb Collaboration, R. Aaij et al., Measurement of B meson production cross-sections in proton–proton collisions at $\sqrt{s} = 7$ TeV. JHEP **08**, 117 (2013). arXiv:1306.3663 [hep-ex]

44. CMS Collaboration, S. Chatrchyan et al., Measurement of the strange B meson production cross section with J/Psi ϕ decays in *pp* collisions at $\sqrt{s} = 7$ TeV. Phys. Rev. D **84**, 052008 (2011). arXiv:1106.4048 [hep-ex]

45. CMS Collaboration, V. Khachatryan et al., Measurement of the B^+ production cross section in pp collisions at $\sqrt{s} = 7$ TeV. Phys. Rev. Lett. **106**, 112001 (2011). arXiv:1101.0131 [hep-ex]

46. CMS Collaboration, S. Chatrchyan et al., Measurement of the B^0 production cross section in *pp* collisions at $\sqrt{s} = 7$ TeV. Phys. Rev. Lett. **106**, 252001 (2011). arXiv:1104.2892 [hep-ex]

47. ALICE Collaboration, B. Abelev et al., Measurement of electrons from beauty hadron decays in *pp* collisions at $\sqrt{s} = 7$ TeV. Phys. Lett. B **721**, 13–23 (2013). arXiv:1208.1902 [hep-ex]

48. ALICE Collaboration, B. Abelev et al., Measurement of prompt J/ψ and beauty hadron production cross sections at mid-rapidity in *pp* collisions at $\sqrt{s} = 7$ TeV. JHEP **11**, 065 (2012). arXiv:1205.5880 [hep-ex]

49. J. Pumplin, D.R. Stump, J. Huston, H.L. Lai, P.M. Nadolsky, W.K. Tung, New generation of parton distributions with uncertainties from global QCD analysis. JHEP **07**, 012 (2002). arXiv:hep-ph/0201195 [hep-ph]

50. L.A. Harland-Lang, A.D. Martin, P. Motylinski, R.S. Thorne, Parton distributions in the LHC era: MMHT 2014 PDFs. Eur. Phys. J. C **75**(5), 204 (2015). arXiv:1412.3989 [hep-ph]

51. L. Gladilin, Fragmentation fractions of *c* and *b* quarks into charmed hadrons at LEP. Eur. Phys. J. C **75**(1), 19 (2015). arXiv:1404.3888 [hep-ex]

52. T. Kneesch, B.A. Kniehl, G. Kramer, I. Schienbein, Charmed-meson fragmentation functions with finite-mass corrections. Nucl. Phys. B **799**, 34–59 (2008). arXiv:0712.0481 [hep-ph]

53. M. Cacciari, P. Nason, Charm cross-sections for the Tevatron Run II. JHEP **09**, 006 (2003). arXiv:hep-ph/0306212 [hep-ph]

54. ALEPH Collaboration, R. Barate et al., Study of charm production in Z decays. Eur. Phys. J. C **16**, 597–611 (2000). arXiv:hep-ex/9909032 [hep-ex]

55. B.A. Kniehl, G. Kramer, Charmed-hadron fragmentation functions from CERN LEP1 revisited. Phys. Rev. D **74**, 037502 (2006). arXiv:hep-ph/0607306 [hep-ph]

56. C. Peterson, D. Schlatter, I. Schmitt, P.M. Zerwas, Scaling violations in inclusive e+ e- annihilation spectra. Phys. Rev. D **27**, 105 (1983)

57. E. Braaten, K.-M. Cheung, S. Fleming, T.C. Yuan, Perturbative QCD fragmentation functions as a model for heavy quark fragmentation. Phys. Rev. D **51**, 4819–4829 (1995). arXiv:hep-ph/9409316 [hep-ph]

58. M.L. Mangano, P. Nason, G. Ridolfi, Heavy quark correlations in hadron collisions at next-to-leading order. Nucl. Phys. B **373**, 295–345 (1992)

59. S. Frixione, P. Nason, G. Ridolfi, A positive-weight next-to-leading-order Monte Carlo for heavy flavour hadroproduction. JHEP **09**, 126 (2007). arXiv:0707.3088 [hep-ph]

60. ZEUS Collaboration, H. Abramowicz et al., Measurement of charm fragmentation fractions in photoproduction at HERA. JHEP **09**, 058 (2013). arXiv:1306.4862 [hep-ex]

61. M. Lisovyi, A. Verbytskyi, O. Zenaiev, Combined analysis of charm-quark fragmentation-fraction measurements. Eur. Phys. J. C **76**(7), 397 (2016). arXiv:1509.01061 [hep-ex]

ALICE Collaboration

S. Acharya[139], D. Adamová[87], M. M. Aggarwal[91], G. Aglieri Rinella[34], M. Agnello[30], N. Agrawal[47], Z. Ahammed[139], N. Ahmad[17], S. U. Ahn[69], S. Aiola[143], A. Akindinov[54], S. N. Alam[139], D. S. D. Albuquerque[124], D. Aleksandrov[83], B. Alessandro[113], D. Alexandre[104], R. Alfaro Molina[64], A. Alici[12,26,107], A. Alkin[3], J. Alme[21], T. Alt[41], I. Altsybeev[138], C. Alves Garcia Prado[123], M. An[7], C. Andrei[80], H. A. Andrews[104], A. Andronic[100], V. Anguelov[96], C. Anson[90], T. Antičić[101], F. Antinori[110], P. Antonioli[107], R. Anwar[126], L. Aphecetche[116], H. Appelshäuser[60], S. Arcelli[26], R. Arnaldi[113], O. W. Arnold[35,97], I. C. Arsene[20], M. Arslandok[60], B. Audurier[116], A. Augustinus[34], R. Averbeck[100], M. D. Azmi[17], A. Badalà[109], Y. W. Baek[68], S. Bagnasco[113], R. Bailhache[60], R. Bala[93], A. Baldisseri[65], M. Ball[44], R. C. Baral[57], A. M. Barbano[25], R. Barbera[27], F. Barile[32,106], L. Barioglio[25], G. G. Barnaföldi[142], L. S. Barnby[34,104], V. Barret[71], P. Bartalini[7], K. Barth[34], J. Bartke[120,a], E. Bartsch[60], M. Basile[26], N. Bastid[71], S. Basu[139], B. Bathen[61], G. Batigne[116], A. Batista Camejo[71], B. Batyunya[67], P. C. Batzing[20], I. G. Bearden[84], H. Beck[96], C. Bedda[30], N. K. Behera[50], I. Belikov[135], F. Bellini[26], H. Bello Martinez[2], R. Bellwied[126], L. G. E. Beltran[122], V. Belyaev[76], G. Bencedi[142], S. Beole[25], A. Bercuci[80], Y. Berdnikov[89], D. Berenyi[142], R. A. Bertens[53,129], D. Berzano[34], L. Betev[34], A. Bhasin[93], I. R. Bhat[93], A. K. Bhati[91], B. Bhattacharjee[43], J. Bhom[120], L. Bianchi[126], N. Bianchi[73], C. Bianchin[141], J. Bielčík[38], J. Bielčíková[87], A. Bilandzic[35,97], G. Biro[142], R. Biswas[4], S. Biswas[4], J. T. Blair[121], D. Blau[83], C. Blume[60], G. Boca[136], F. Bock[75,96], A. Bogdanov[76], L. Boldizsár[142], M. Bombara[39], G. Bonomi[137], M. Bonora[34], J. Book[60], H. Borel[65], A. Borissov[99], M. Borri[128], E. Botta[25], C. Bourjau[84], P. Braun-Munzinger[100], M. Bregant[123], T. A. Broker[60], T. A. Browning[98], M. Broz[38], E. J. Brucken[45], E. Bruna[113], G. E. Bruno[32], D. Budnikov[102], H. Buesching[60], S. Bufalino[30], P. Buhler[115], S. A. I. Buitron[62], P. Buncic[34], O. Busch[132], Z. Buthelezi[66], J. B. Butt[15], J. T. Buxton[18], J. Cabala[118], D. Caffarri[34], H. Caines[143], A. Caliva[53], E. Calvo Villar[105], P. Camerini[24], A. A. Capon[115], F. Carena[34], W. Carena[34], F. Carnesecchi[12,26], J. Castillo Castellanos[65], A. J. Castro[129], E. A. R. Casula[23,108], C. Ceballos Sanchez[9], P. Cerello[113], B. Chang[127], S. Chapeland[34], M. Chartier[128], J. L. Charvet[65], S. Chattopadhyay[139], S. Chattopadhyay[103], A. Chauvin[97,35], M. Cherney[90], C. Cheshkov[134], B. Cheynis[134], V. Chibante Barroso[34], D. D. Chinellato[124], S. Cho[50], P. Chochula[34], K. Choi[99], M. Chojnacki[84], S. Choudhury[139], P. Christakoglou[85], C. H. Christensen[84], P. Christiansen[33], T. Chujo[132], S. U. Chung[99], C. Cicalo[108], L. Cifarelli[12,26], F. Cindolo[107], J. Cleymans[92], F. Colamaria[32], D. Colella[34,55], A. Collu[75], M. Colocci[26], M. Concas[113,b], G. Conesa Balbastre[72], Z. Conesa del Valle[51], M. E. Connors[143,c], J. G. Contreras[38], T. M. Cormier[88], Y. Corrales Morales[113], I. Cortés Maldonado[2], P. Cortese[31], M. R. Cosentino[125], F. Costa[34], S. Costanza[136], J. Crkovská[51], P. Crochet[71], E. Cuautle[62], L. Cunqueiro[61], T. Dahms[35,97], A. Dainese[110], M. C. Danisch[96], A. Danu[58], D. Das[103], I. Das[103], S. Das[4], A. Dash[81], S. Dash[47], S. De[48,123], A. De Caro[29], G. de Cataldo[106], C. de Conti[123], J. de Cuveland[41], A. De Falco[23], D. De Gruttola[12,29], N. De Marco[113], S. De Pasquale[29], R. D. De Souza[124], H. F. Degenhardt[123], A. Deisting[96,100], A. Deloff[79], C. Deplano[85], P. Dhankher[47], D. Di Bari[32], A. Di Mauro[34], P. Di Nezza[73], B. Di Ruzza[110], M. A. Diaz Corchero[10], T. Dietel[92], P. Dillenseger[60], R. Divià[34], Ø. Djuvsland[21], A. Dobrin[58,34], D. Domenicis Gimenez[123], B. Dönigus[60], O. Dordic[20], T. Drozhzhova[60], A. K. Dubey[139], A. Dubla[100], L. Ducroux[134], A. K. Duggal[91], P. Dupieux[71], R. J. Ehlers[143], D. Elia[106], E. Endress[105], H. Engel[59], E. Epple[143], B. Erazmus[116], F. Erhardt[133], B. Espagnon[51], S. Esumi[132], G. Eulisse[34], J. Eum[99], D. Evans[104], S. Evdokimov[114], L. Fabbietti[35,97], J. Faivre[72], A. Fantoni[73], M. Fasel[75,88], L. Feldkamp[61], A. Feliciello[113], G. Feofilov[138], J. Ferencei[87], A. Fernández Téllez[2], E. G. Ferreiro[16], A. Ferretti[25], A. Festanti[28], V. J. G. Feuillard[65,71], J. Figiel[120], M. A. S. Figueredo[123], S. Filchagin[102], D. Finogeev[52], F. M. Fionda[23], E. M. Fiore[32], M. Floris[34], S. Foertsch[66], P. Foka[100], S. Fokin[83], E. Fragiacomo[112], A. Francescon[34], A. Francisco[116], U. Frankenfeld[100], G. G. Fronze[25], U. Fuchs[34], C. Furget[72], A. Furs[52], M. Fusco Girard[29], J. J. Gaardhøje[84], M. Gagliardi[25], A. M. Gago[105], K. Gajdosova[84], M. Gallio[25], C. D. Galvan[122], P. Ganoti[78], C. Gao[7], C. Garabatos[100], E. Garcia-Solis[13], K. Garg[27], P. Garg[48], C. Gargiulo[34], P. Gasik[97,35], E. F. Gauger[121], M. B. Gay Ducati[63], M. Germain[116], P. Ghosh[139], S. K. Ghosh[4], P. Gianotti[73], P. Giubellino[34,113], P. Giubilato[28], E. Gladysz-Dziadus[120],

P. Glässel[96],   D. M. Goméz Coral[64],   A. Gomez Ramirez[59],   A. S. Gonzalez[34],   V. Gonzalez[10],   P. González-Zamora[10], S. Gorbunov[41],   L. Görlich[120],   S. Gotovac[119],   V. Grabski[64],   L. K. Graczykowski[140],   K. L. Graham[104],   L. Greiner[75], A. Grelli[53],   C. Grigoras[34],   V. Grigoriev[76],   A. Grigoryan[1],   S. Grigoryan[67],   N. Grion[112],   J. M. Gronefeld[100],   F. Grosa[30], J. F. Grosse-Oetringhaus[34],   R. Grosso[100],   L. Gruber[115],   F. R. Grull[59],   F. Guber[52],   R. Guernane[72],   B. Guerzoni[26], K. Gulbrandsen[84],   T. Gunji[131],   A. Gupta[93],   R. Gupta[93],   I. B. Guzman[2],   R. Haake[34],   C. Hadjidakis[51],   H. Hamagaki[77,131], G. Hamar[142],   J. C. Hamon[135],   J. W. Harris[143],   A. Harton[13],   D. Hatzifotiadou[107],   S. Hayashi[131],   S. T. Heckel[60], E. Hellbär[60],   H. Helstrup[36],   A. Herghelegiu[80],   G. Herrera Corral[11],   F. Herrmann[61],   B. A. Hess[95],   K. F. Hetland[36], H. Hillemanns[34],   B. Hippolyte[135],   J. Hladky[56],   B. Hohlweger[97],   D. Horak[38],   R. Hosokawa[132],   P. Hristov[34],   C. Hughes[129], T. J. Humanic[18],   N. Hussain[43],   T. Hussain[17],   D. Hutter[41],   D. S. Hwang[19],   R. Ilkaev[102],   M. Inaba[132],   M. Ippolitov[76,83], M. Irfan[17],   V. Isakov[52],   M. S. Islam[48],   M. Ivanov[34,100],   V. Ivanov[89],   V. Izucheev[114],   B. Jacak[75],   N. Jacazio[26], P. M. Jacobs[75],   M. B. Jadhav[47],   S. Jadlovska[118],   J. Jadlovsky[118],   S. Jaelani[53],   C. Jahnke[35],   M. J. Jakubowska[140], M. A. Janik[140],   P. H. S. Y. Jayarathna[126],   C. Jena[81],   S. Jena[126],   M. Jercic[133],   R. T. Jimenez Bustamante[100],   P. G. Jones[104], A. Jusko[104],   P. Kalinak[55],   A. Kalweit[34],   J. H. Kang[144],   V. Kaplin[76],   S. Kar[139],   A. Karasu Uysal[70],   O. Karavichev[52], T. Karavicheva[52],   L. Karayan[96,100],   E. Karpechev[52],   U. Kebschull[59],   R. Keidel[145],   D. L. D. Keijdener[53],   M. Keil[34], B. Ketzer[44],   M. Mohisin Khan[17,d],   P. Khan[103],   S. A. Khan[139],   A. Khanzadeev[89],   Y. Kharlov[114],   A. Khatun[17],   A. Khuntia[48], M. M. Kielbowicz[120],   B. Kileng[36],   D. Kim[144],   D. W. Kim[42],   D. J. Kim[127],   H. Kim[144],   J. S. Kim[42],   J. Kim[96],   M. Kim[50], M. Kim[144],   S. Kim[19],   T. Kim[144],   S. Kirsch[41],   I. Kisel[41],   S. Kiselev[54],   A. Kisiel[140],   G. Kiss[142],   J. L. Klay[6],   C. Klein[60], J. Klein[34],   C. Klein-Bösing[61],   S. Klewin[96],   A. Kluge[34],   M. L. Knichel[96],   A. G. Knospe[126],   C. Kobdaj[117],   M. Kofarago[34], T. Kollegger[100],   A. Kolojvari[138],   V. Kondratiev[138],   N. Kondratyeva[76],   E. Kondratyuk[114],   A. Konevskikh[52],   M. Kopcik[118], M. Kour[93],   C. Kouzinopoulos[34],   O. Kovalenko[79],   V. Kovalenko[138],   M. Kowalski[120],   G. Koyithatta Meethaleveedu[47], I. Králik[55],   A. Kravčáková[39],   M. Krivda[55,104],   F. Krizek[87],   E. Kryshen[89],   M. Krzewicki[41],   A. M. Kubera[18],   V. Kučera[87], C. Kuhn[135],   P. G. Kuijer[85],   A. Kumar[93],   J. Kumar[47],   L. Kumar[91],   S. Kumar[47],   S. Kundu[81],   P. Kurashvili[79],   A. Kurepin[52], A. B. Kurepin[52],   A. Kuryakin[102],   S. Kushpil[87],   M. J. Kweon[50],   Y. Kwon[144],   S. L. La Pointe[41],   P. La Rocca[27], C. Lagana Fernandes[123],   I. Lakomov[34],   R. Langoy[40],   K. Lapidus[143],   C. Lara[59],   A. Lardeux[20,65],   A. Lattuca[25], E. Laudi[34],   R. Lavicka[38],   L. Lazaridis[34],   R. Lea[24],   L. Leardini[96],   S. Lee[144],   F. Lehas[85],   S. Lehner[115],   J. Lehrbach[41], R. C. Lemmon[86],   V. Lenti[106],   E. Leogrande[53],   I. León Monzón[122],   P. Lévai[142],   S. Li[7],   X. Li[14],   J. Lien[40],   R. Lietava[104], S. Lindal[20],   V. Lindenstruth[41],   C. Lippmann[100],   M. A. Lisa[18],   V. Litichevskyi[45],   H. M. Ljunggren[33],   W. J. Llope[141], D. F. Lodato[53],   P. I. Loenne[21],   V. Loginov[76],   C. Loizides[75],   P. Loncar[119],   X. Lopez[71],   E. López Torres[9],   A. Lowe[142], P. Luettig[60],   M. Lunardon[28],   G. Luparello[24],   M. Lupi[34],   T. H. Lutz[143],   A. Maevskaya[52],   M. Mager[34],   S. Mahajan[93], S. M. Mahmood[20], A. Maire[135], R. D. Majka[143], M. Malaev[89], I. Maldonado Cervantes[62], L. Malinina[67,e], D. Mal'Kevich[54], P. Malzacher[100],   A. Mamonov[102],   V. Manko[83],   F. Manso[71],   V. Manzari[106],   Y. Mao[7],   M. Marchisone[66,130],   J. Mareš[56], G. V. Margagliotti[24],   A. Margotti[107],   J. Margutti[53],   A. Marín[100],   C. Markert[121],   M. Marquard[60],   N. A. Martin[100], P. Martinengo[34],   J. A. L. Martinez[59],   M. I. Martínez[2],   G. Martínez García[116],   M. Martinez Pedreira[34],   A. Mas[123], S. Masciocchi[100],   M. Masera[25],   A. Masoni[108],   A. Mastroserio[32],   A. M. Mathis[35,97],   A. Matyja[120,129],   C. Mayer[120], J. Mazer[129],   M. Mazzilli[32],   M. A. Mazzoni[111],   F. Meddi[22],   Y. Melikyan[76],   A. Menchaca-Rocha[64],   E. Meninno[29], J. Mercado Pérez[96],   M. Meres[37],   S. Mhlanga[92],   Y. Miake[132],   M. M. Mieskolainen[45],   D. L. Mihaylov[97],   K. Mikhaylov[54,67], L. Milano[75],   J. Milosevic[20],   A. Mischke[53],   A. N. Mishra[48],   D. Miśkowiec[100],   J. Mitra[139],   C. M. Mitu[58],   N. Mohammadi[53], B. Mohanty[81],   E. Montes[10],   D. A. Moreira De Godoy[61],   L. A. P. Moreno[2],   S. Moretto[28],   A. Morreale[116],   A. Morsch[34], V. Muccifora[73],   E. Mudnic[119],   D. Mühlheim[61],   S. Muhuri[139],   M. Mukherjee[4,139],   J. D. Mulligan[143],   M. G. Munhoz[123], K. Münning[44],   R. H. Munzer[60],   H. Murakami[131],   S. Murray[66],   L. Musa[34],   J. Musinsky[55],   C. J. Myers[126],   B. Naik[47], R. Nair[79],   B. K. Nandi[47],   R. Nania[107],   E. Nappi[106],   M. U. Naru[15],   H. Natal da Luz[123],   C. Nattrass[129],   S. R. Navarro[2], K. Nayak[81],   R. Nayak[47],   T. K. Nayak[139],   S. Nazarenko[102],   A. Nedosekin[54],   R. A. Negrao De Oliveira[34],   L. Nellen[62], S. V. Nesbo[36],   F. Ng[126],   M. Nicassio[100],   M. Niculescu[58],   J. Niedziela[34],   B. S. Nielsen[84],   S. Nikolaev[83],   S. Nikulin[83], V. Nikulin[89],   F. Noferini[12,107],   P. Nomokonov[67],   G. Nooren[53],   J. C. C. Noris[2],   J. Norman[128],   A. Nyanin[83],   J. Nystrand[21], H. Oeschler[96,a],   S. Oh[143],   A. Ohlson[34,96],   T. Okubo[46],   L. Olah[142],   J. Oleniacz[140],   A. C. Oliveira Da Silva[123], M. H. Oliver[143],   J. Onderwaater[100],   C. Oppedisano[113],   R. Orava[45],   M. Oravec[118],   A. Ortiz Velasquez[62],   A. Oskarsson[33], J. Otwinowski[120],   K. Oyama[77],   Y. Pachmayer[96],   V. Pacik[84],   D. Pagano[137],   P. Pagano[29],   G. Paić[62],   P. Palni[7],   J. Pan[141], A. K. Pandey[47],   S. Panebianco[65],   V. Papikyan[1],   G. S. Pappalardo[109],   P. Pareek[48],   J. Park[50],   W. J. Park[100],   S. Parmar[91], A. Passfeld[61],   S. P. Pathak[126],   V. Paticchio[106],   R. N. Patra[139],   B. Paul[113],   H. Pei[7],   T. Peitzmann[53],   X. Peng[7], L. G. Pereira[63],   H. Pereira Da Costa[65],   D. Peresunko[76,83],   E. Perez Lezama[60],   V. Peskov[60],   Y. Pestov[5],   V. Petráček[38], V. Petrov[114],   M. Petrovici[80],   C. Petta[27],   R. P. Pezzi[63],   S. Piano[112],   M. Pikna[37],   P. Pillot[116],   L. O. D. L. Pimentel[84], O. Pinazza[34,107],   L. Pinsky[126],   D. B. Piyarathna[126],   M. Płoskoń[75],   M. Planinic[133],   J. Pluta[140],   S. Pochybova[142], P. L. M. Podesta-Lerma[122],   M. G. Poghosyan[88],   B. Polichtchouk[114],   N. Poljak[133],   W. Poonsawat[117],   A. Pop[80],

H. Poppenborg[61], S. Porteboeuf-Houssais[71], J. Porter[75], J. Pospisil[87], V. Pozdniakov[67], S. K. Prasad[4], R. Preghenella[34,107], F. Prino[113], C. A. Pruneau[141], I. Pshenichnov[52], M. Puccio[25], G. Puddu[23], P. Pujahari[141], V. Punin[102], J. Putschke[141], H. Qvigstad[20], A. Rachevski[112], S. Raha[4], S. Rajput[93], J. Rak[127], A. Rakotozafindrabe[65], L. Ramello[31], F. Rami[135], D. B. Rana[126], R. Raniwala[94], S. Raniwala[94], S. S. Räsänen[45], B. T. Rascanu[60], D. Rathee[91], V. Ratza[44], I. Ravasenga[30], K. F. Read[88,129], K. Redlich[79], A. Rehman[21], P. Reichelt[60], F. Reidt[34], X. Ren[7], R. Renfordt[60], A. R. Reolon[73], A. Reshetin[52], K. Reygers[96], V. Riabov[89], R. A. Ricci[74], T. Richert[33,53], M. Richter[20], P. Riedler[34], W. Riegler[34], F. Riggi[27], C. Ristea[58], M. Rodríguez Cahuantzi[2], K. Røed[20], E. Rogochaya[67], D. Rohr[41], D. Röhrich[21], P. S. Rokita[140], F. Ronchetti[34,73], L. Ronflette[116], P. Rosnet[71], A. Rossi[28], A. Rotondi[136], F. Roukoutakis[78], A. Roy[48], C. Roy[135], P. Roy[103], A. J. Rubio Montero[10], O. V. Rueda[62], R. Rui[24], R. Russo[25], A. Rustamov[82], E. Ryabinkin[83], Y. Ryabov[89], A. Rybicki[120], S. Saarinen[45], S. Sadhu[139], S. Sadovsky[114], K. Šafařík[34], S. K. Saha[139], B. Sahlmuller[60], B. Sahoo[47], P. Sahoo[48], R. Sahoo[48], S. Sahoo[57], P. K. Sahu[57], J. Saini[139], S. Sakai[73,132], M. A. Saleh[141], J. Salzwedel[18], S. Sambyal[93], V. Samsonov[76,89], A. Sandoval[64], D. Sarkar[139], N. Sarkar[139], P. Sarma[43], M. H. P. Sas[53], E. Scapparone[107], F. Scarlassara[28], R. P. Scharenberg[98], H. S. Scheid[60], C. Schiaua[80], R. Schicker[96], C. Schmidt[100], H. R. Schmidt[95], M. O. Schmidt[96], M. Schmidt[95], S. Schuchmann[60], J. Schukraft[34], Y. Schutz[34,116,135], K. Schwarz[100], K. Schweda[100], G. Scioli[26], E. Scomparin[113], R. Scott[129], M. Šefčík[39], J. E. Seger[90], Y. Sekiguchi[131], D. Sekihata[46], I. Selyuzhenkov[100], K. Senosi[66], S. Senyukov[3,34,135], E. Serradilla[10,64], P. Sett[47], A. Sevcenco[58], A. Shabanov[52], A. Shabetai[116], O. Shadura[3], R. Shahoyan[34], A. Shangaraev[114], A. Sharma[91], A. Sharma[93], M. Sharma[93], M. Sharma[93], N. Sharma[91,129], A. I. Sheikh[139], K. Shigaki[46], Q. Shou[7], K. Shtejer[9,25], Y. Sibiriak[83], S. Siddhanta[108], K. M. Sielewicz[34], T. Siemiarczuk[79], D. Silvermyr[33], C. Silvestre[72], G. Simatovic[133], G. Simonetti[34], R. Singaraju[139], R. Singh[81], V. Singhal[139], T. Sinha[103], B. Sitar[37], M. Sitta[31], T. B. Skaali[20], M. Slupecki[127], N. Smirnov[143], R. J. M. Snellings[53], T. W. Snellman[127], J. Song[99], M. Song[144], F. Soramel[28], S. Sorensen[129], F. Sozzi[100], E. Spiriti[73], I. Sputowska[120], B. K. Srivastava[98], J. Stachel[96], I. Stan[58], P. Stankus[88], E. Stenlund[33], J. H. Stiller[96], D. Stocco[116], P. Strmen[37], A. A. P. Suaide[123], T. Sugitate[46], C. Suire[51], M. Suleymanov[15], M. Suljic[24], R. Sultanov[54], M. Šumbera[87], S. Sumowidagdo[49], K. Suzuki[115], S. Swain[57], A. Szabo[37], I. Szarka[37], A. Szczepankiewicz[140], M. Szymanski[140], U. Tabassam[15], J. Takahashi[124], G. J. Tambave[21], N. Tanaka[132], M. Tarhini[51], M. Tariq[17], M. G. Tarzila[80], A. Tauro[34], G. Tejeda Muñoz[2], A. Telesca[34], K. Terasaki[131], C. Terrevoli[28], B. Teyssier[134], D. Thakur[48], S. Thakur[139], D. Thomas[121], R. Tieulent[134], A. Tikhonov[52], A. R. Timmins[126], A. Toia[60], S. Tripathy[48], S. Trogolo[25], G. Trombetta[32], V. Trubnikov[3], W. H. Trzaska[127], B. A. Trzeciak[53], T. Tsuji[131], A. Tumkin[102], R. Turrisi[110], T. S. Tveter[20], K. Ullaland[21], E. N. Umaka[126], A. Uras[134], G. L. Usai[23], A. Utrobicic[133], M. Vala[55,118], J. Van Der Maarel[53], J. W. Van Hoorne[34], M. van Leeuwen[53], T. Vanat[87], P. Vande Vyvre[34], D. Varga[142], A. Vargas[2], M. Vargyas[127], R. Varma[47], M. Vasileiou[78], A. Vasiliev[83], A. Vauthier[72], O. Vázquez Doce[35,97], V. Vechernin[138], A. M. Veen[53], A. Velure[21], E. Vercellin[25], S. Vergara Limón[2], R. Vernet[8], R. Vértesi[142], L. Vickovic[119], S. Vigolo[53], J. Viinikainen[127], Z. Vilakazi[130], O. Villalobos Baillie[104], A. Villatoro Tello[2], A. Vinogradov[83], L. Vinogradov[138], T. Virgili[29], V. Vislavicius[33], A. Vodopyanov[67], M. A. Völkl[96], K. Voloshin[54], S. A. Voloshin[141], G. Volpe[32], B. von Haller[34], I. Vorobyev[35,97], D. Voscek[118], D. Vranic[34,100], J. Vrláková[39], B. Wagner[21], J. Wagner[100], H. Wang[53], M. Wang[7], D. Watanabe[132], Y. Watanabe[131], M. Weber[115], S. G. Weber[100], D. F. Weiser[96], J. P. Wessels[61], U. Westerhoff[61], A. M. Whitehead[92], J. Wiechula[60], J. Wikne[20], G. Wilk[79], J. Wilkinson[96], G. A. Willems[61], M. C. S. Williams[107], B. Windelband[96], W. E. Witt[129], S. Yalcin[70], P. Yang[7], S. Yano[46], Z. Yin[7], H. Yokoyama[72,132], I.-K. Yoo[34,99], J. H. Yoon[50], V. Yurchenko[3], V. Zaccolo[84,113], A. Zaman[15], C. Zampolli[34], H. J. C. Zanoli[123], N. Zardoshti[104], A. Zarochentsev[138], P. Závada[56], N. Zaviyalov[102], H. Zbroszczyk[140], M. Zhalov[89], H. Zhang[7,21], X. Zhang[7], Y. Zhang[7], C. Zhang[53], Z. Zhang[7], C. Zhao[20], N. Zhigareva[54], D. Zhou[7], Y. Zhou[84], Z. Zhou[21], H. Zhu[7,21], J. Zhu[7,116], X. Zhu[7], A. Zichichi[12,26], A. Zimmermann[96], M. B. Zimmermann[34,61], S. Zimmermann[115], G. Zinovjev[3], J. Zmeskal[115]

[1] A.I. Alikhanyan National Science Laboratory (Yerevan Physics Institute) Foundation, Yerevan, Armenia
[2] Benemérita Universidad Autónoma de Puebla, Puebla, Mexico
[3] Bogolyubov Institute for Theoretical Physics, Kiev, Ukraine
[4] Department of Physics and Centre for Astroparticle Physics and Space Science (CAPSS), Bose Institute, Kolkata, India
[5] Budker Institute for Nuclear Physics, Novosibirsk, Russia
[6] California Polytechnic State University, San Luis Obispo, CA, USA
[7] Central China Normal University, Wuhan, China
[8] Centre de Calcul de l'IN2P3, Villeurbanne, Lyon, France
[9] Centro de Aplicaciones Tecnológicas y Desarrollo Nuclear (CEADEN), Havana, Cuba
[10] Centro de Investigaciones Energéticas Medioambientales y Tecnológicas (CIEMAT), Madrid, Spain
[11] Centro de Investigación y de Estudios Avanzados (CINVESTAV), Mexico City, Mérida, Mexico

[12] Centro Fermi-Museo Storico della Fisica e Centro Studi e Ricerche "Enrico Fermi', Rome, Italy

[13] Chicago State University, Chicago, IL, USA

[14] China Institute of Atomic Energy, Beijing, China

[15] COMSATS Institute of Information Technology (CIIT), Islamabad, Pakistan

[16] Departamento de Física de Partículas and IGFAE, Universidad de Santiago de Compostela, Santiago de Compostela, Spain

[17] Department of Physics, Aligarh Muslim University, Aligarh, India

[18] Department of Physics, Ohio State University, Columbus, OH, USA

[19] Department of Physics, Sejong University, Seoul, South Korea

[20] Department of Physics, University of Oslo, Oslo, Norway

[21] Department of Physics and Technology, University of Bergen, Bergen, Norway

[22] Dipartimento di Fisica dell'Università 'La Sapienza' and Sezione INFN, Rome, Italy

[23] Dipartimento di Fisica dell'Università and Sezione INFN, Cagliari, Italy

[24] Dipartimento di Fisica dell'Università and Sezione INFN, Trieste, Italy

[25] Dipartimento di Fisica dell'Università and Sezione INFN, Turin, Italy

[26] Dipartimento di Fisica e Astronomia dell'Università and Sezione INFN, Bologna, Italy

[27] Dipartimento di Fisica e Astronomia dell'Università and Sezione INFN, Catania, Italy

[28] Dipartimento di Fisica e Astronomia dell'Università and Sezione INFN, Padua, Italy

[29] Dipartimento di Fisica 'E.R. Caianiello' dell'Università and Gruppo Collegato INFN, Salerno, Italy

[30] Dipartimento DISAT del Politecnico and Sezione INFN, Turin, Italy

[31] Dipartimento di Scienze e Innovazione Tecnologica dell'Università del Piemonte Orientale and INFN Sezione di Torino, Alessandria, Italy

[32] Dipartimento Interateneo di Fisica 'M. Merlin' and Sezione INFN, Bari, Italy

[33] Division of Experimental High Energy Physics, University of Lund, Lund, Sweden

[34] European Organization for Nuclear Research (CERN), Geneva, Switzerland

[35] Excellence Cluster Universe, Technische Universität München, Munich, Germany

[36] Faculty of Engineering, Bergen University College, Bergen, Norway

[37] Faculty of Mathematics, Physics and Informatics, Comenius University, Bratislava, Slovakia

[38] Faculty of Nuclear Sciences and Physical Engineering, Czech Technical University in Prague, Prague, Czech Republic

[39] Faculty of Science, P.J. Šafárik University, Kosice, Slovakia

[40] Faculty of Technology, Buskerud and Vestfold University College, Tonsberg, Norway

[41] Frankfurt Institute for Advanced Studies, Johann Wolfgang Goethe-Universität Frankfurt, Frankfurt, Germany

[42] Gangneung-Wonju National University, Gangneung, South Korea

[43] Department of Physics, Gauhati University, Guwahati, India

[44] Helmholtz-Institut für Strahlen- und Kernphysik, Rheinische Friedrich-Wilhelms-Universität Bonn, Bonn, Germany

[45] Helsinki Institute of Physics (HIP), Helsinki, Finland

[46] Hiroshima University, Hiroshima, Japan

[47] Indian Institute of Technology Bombay (IIT), Mumbai, India

[48] Indian Institute of Technology Indore, Indore, India

[49] Indonesian Institute of Sciences, Jakarta, Indonesia

[50] Inha University, Incheon, South Korea

[51] Institut de Physique Nucléaire d'Orsay (IPNO), Université Paris-Sud, CNRS-IN2P3, Orsay, France

[52] Institute for Nuclear Research, Academy of Sciences, Moscow, Russia

[53] Institute for Subatomic Physics of Utrecht University, Utrecht, The Netherlands

[54] Institute for Theoretical and Experimental Physics, Moscow, Russia

[55] Institute of Experimental Physics, Slovak Academy of Sciences, Kosice, Slovakia

[56] Institute of Physics, Academy of Sciences of the Czech Republic, Prague, Czech Republic

[57] Institute of Physics, Bhubaneswar, India

[58] Institute of Space Science (ISS), Bucharest, Romania

[59] Institut für Informatik, Johann Wolfgang Goethe-Universität Frankfurt, Frankfurt, Germany

[60] Institut für Kernphysik, Johann Wolfgang Goethe-Universität Frankfurt, Frankfurt, Germany

[61] Institut für Kernphysik, Westfälische Wilhelms-Universität Münster, Münster, Germany

[62] Instituto de Ciencias Nucleares, Universidad Nacional Autónoma de México, Mexico City, Mexico

[63] Instituto de Física, Universidade Federal do Rio Grande do Sul (UFRGS), Porto Alegre, Brazil

[64] Instituto de Física, Universidad Nacional Autónoma de México, Mexico City, Mexico

[65] IRFU, CEA, Université Paris-Saclay, 91191 Gif-sur-Yvette, Saclay, France

[66] iThemba LABS, National Research Foundation, Somerset West, South Africa

[67] Joint Institute for Nuclear Research (JINR), Dubna, Russia

[68] Konkuk University, Seoul, South Korea

[69] Korea Institute of Science and Technology Information, Daejeon, South Korea

[70] KTO Karatay University, Konya, Turkey

[71] Laboratoire de Physique Corpusculaire (LPC), Clermont Université, Université Blaise Pascal, CNRS-IN2P3, Clermont-Ferrand, France

[72] Laboratoire de Physique Subatomique et de Cosmologie, Université Grenoble-Alpes, CNRS-IN2P3, Grenoble, France

[73] Laboratori Nazionali di Frascati, INFN, Frascati, Italy

[74] Laboratori Nazionali di Legnaro, INFN, Legnaro, Italy

[75] Lawrence Berkeley National Laboratory, Berkeley, CA, USA

[76] Moscow Engineering Physics Institute, Moscow, Russia

[77] Nagasaki Institute of Applied Science, Nagasaki, Japan

[78] Physics Department, National and Kapodistrian University of Athens, Athens, Greece

[79] National Centre for Nuclear Studies, Warsaw, Poland

[80] National Institute for Physics and Nuclear Engineering, Bucharest, Romania

[81] National Institute of Science Education and Research, Bhubaneswar, India

[82] National Nuclear Research Center, Baku, Azerbaijan

[83] National Research Centre Kurchatov Institute, Moscow, Russia

[84] Niels Bohr Institute, University of Copenhagen, Copenhagen, Denmark

[85] Nikhef, Nationaal instituut voor subatomaire fysica, Amsterdam, The Netherlands

[86] Nuclear Physics Group, STFC Daresbury Laboratory, Daresbury, UK

[87] Nuclear Physics Institute, Academy of Sciences of the Czech Republic, Řež u Prahy, Czech Republic

[88] Oak Ridge National Laboratory, Oak Ridge, TN, USA

[89] Petersburg Nuclear Physics Institute, Gatchina, Russia

[90] Physics Department, Creighton University, Omaha, NE, USA

[91] Physics Department, Panjab University, Chandigarh, India

[92] Physics Department, University of Cape Town, Cape Town, South Africa

[93] Physics Department, University of Jammu, Jammu, India

[94] Physics Department, University of Rajasthan, Jaipur, India

[95] Physikalisches Institut, Eberhard Karls Universität Tübingen, Tübingen, Germany

[96] Physikalisches Institut, Ruprecht-Karls-Universität Heidelberg, Heidelberg, Germany

[97] Physik Department, Technische Universität München, Munich, Germany

[98] Purdue University, West Lafayette, IN, USA

[99] Pusan National University, Pusan, South Korea

[100] Research Division and ExtreMe Matter Institute EMMI, GSI Helmholtzzentrum für Schwerionenforschung GmbH, Darmstadt, Germany

[101] Rudjer Bošković Institute, Zagreb, Croatia

[102] Russian Federal Nuclear Center (VNIIEF), Sarov, Russia

[103] Saha Institute of Nuclear Physics, Kolkata, India

[104] School of Physics and Astronomy, University of Birmingham, Birmingham, UK

[105] Sección Física, Departamento de Ciencias, Pontificia Universidad Católica del Perú, Lima, Peru

[106] Sezione INFN, Bari, Italy

[107] Sezione INFN, Bologna, Italy

[108] Sezione INFN, Cagliari, Italy

[109] Sezione INFN, Catania, Italy

[110] Sezione INFN, Padua, Italy

[111] Sezione INFN, Rome, Italy

[112] Sezione INFN, Trieste, Italy

[113] Sezione INFN, Turin, Italy

[114] SSC IHEP of NRC Kurchatov Institute, Protvino, Russia

[115] Stefan Meyer Institut für Subatomare Physik (SMI), Vienna, Austria

[116] SUBATECH, IMT Atlantique, Université de Nantes, CNRS-IN2P3, Nantes, France

[117] Suranaree University of Technology, Nakhon Ratchasima, Thailand

[118] Technical University of Košice, Kosice, Slovakia

[119] Technical University of Split FESB, Split, Croatia

[120] The Henryk Niewodniczanski Institute of Nuclear Physics, Polish Academy of Sciences, Cracow, Poland

[121] Physics Department, The University of Texas at Austin, Austin, TX, USA

[122] Universidad Autónoma de Sinaloa, Culiacán, Mexico

[123] Universidade de São Paulo (USP), São Paulo, Brazil

[124] Universidade Estadual de Campinas (UNICAMP), Campinas, Brazil

[125] Universidade Federal do ABC, Santo Andre, Brazil

[126] University of Houston, Houston, TX, USA

[127] University of Jyväskylä, Jyväskylä, Finland

[128] University of Liverpool, Liverpool, UK

[129] University of Tennessee, Knoxville, TN, USA

[130] University of the Witwatersrand, Johannesburg, South Africa

[131] University of Tokyo, Tokyo, Japan

[132] University of Tsukuba, Tsukuba, Japan

[133] University of Zagreb, Zagreb, Croatia

[134] Université de Lyon, Université Lyon 1, CNRS/IN2P3, IPN-Lyon, Villeurbanne, Lyon, France

[135] Université de Strasbourg, CNRS, IPHC UMR 7178, 67000 Strasbourg, France

[136] Università degli Studi di Pavia, Pavia, Italy

[137] Università di Brescia, Brescia, Italy

[138] V. Fock Institute for Physics, St. Petersburg State University, St. Petersburg, Russia

[139] Variable Energy Cyclotron Centre, Kolkata, India

[140] Warsaw University of Technology, Warsaw, Poland

[141] Wayne State University, Detroit, MI, USA

[142] Wigner Research Centre for Physics, Hungarian Academy of Sciences, Budapest, Hungary

[143] Yale University, New Haven, CT, USA

[144] Yonsei University, Seoul, South Korea

[145] Zentrum für Technologietransfer und Telekommunikation (ZTT), Fachhochschule Worms, Worms, Germany

[a] Deceased

[b] Also at: Dipartimento DET del Politecnico di Torino, Turin, Italy

[c] Also at: Georgia State University, Atlanta, GA, USA

[d] Also at: Also at Department of Applied Physics, Aligarh Muslim University, Aligarh, India

[e] Also at: M.V. Lomonosov Moscow State University, D.V. Skobeltsyn Institute of Nuclear, Physics, Moscow, Russia